

## REVISED FILTER PROFILES AND ZERO POINTS FOR BROADBAND PHOTOMETRY

ANDREW W. MANN<sup>1,2</sup>, KASPAR VON BRAUN<sup>3,4</sup>

*Accepted to PASP*

### ABSTRACT

Estimating accurate bolometric fluxes for stars requires reliable photometry to absolutely flux calibrate the spectra. This is a significant problem for studies of very bright stars, which are generally saturated in modern photometric surveys. Instead we must rely on photometry with less precise calibration. We utilize precisely flux-calibrated spectra to derive improved filter bandpasses and zero points for the most common sources of photometry for bright stars. In total we test 39 different filters in the General Catalog of Photometric Data as well as those from Tycho-2 and *Hipparcos*. We show that utilizing inaccurate filter profiles from the literature can create significant color terms resulting in fluxes that deviate by  $\gtrsim 10\%$  from actual values. To remedy this we employ an empirical approach; we iteratively adjust the literature filter profile and zero point, convolve it with catalog spectra, and compare to the corresponding flux from the photometry. We adopt the passband values that produces the best agreement between photometry and spectroscopy and is independent of stellar color. We find that while most zero points change by  $< 5\%$ , a few systems change by 10–15%. Our final profiles and zero points are similar to recent estimates from the literature. Based on determinations of systematic errors in our selected spectroscopic libraries, we estimate that most of our improved zero points are accurate to 0.5–1% or better.

*Subject headings:* techniques: spectroscopic — techniques: photometric — stars: fundamental parameters — methods: calibration

### 1. INTRODUCTION

Stellar effective temperatures ( $T_{\text{eff}}$ ) are generally determined through a variety of indirect methods, such as the infrared flux method (IRFM, Blackwell & Shallis 1977; Casagrande et al. 2006, 2010), fitting observations to synthetic spectra (e.g., Valenti & Piskunov 1996), or using equivalent widths and/or line ratios (e.g., Sneden 1973; Sousa et al. 2010, 2011). Because of model errors and the need for a zero point for IRFM these methods must be calibrated using direct methods. The principal direct method is interferometry, which can be used to determine a star’s angular diameter ( $\theta$ ). With  $\theta$  and a measurement of the star’s bolometric flux ( $F_{\text{bol}}$ ) we can calculate effective temperature from a rewritten form of the Stefan-Boltzmann Law:

$$T_{\text{eff}} = \left( \frac{F_{\text{bol}}}{\sigma(\theta/2)^2} \right)^{1/4}, \quad (1)$$

where  $\sigma$  is the Boltzmann constant. Because Equation 1 defines  $T_{\text{eff}}$ , it provides an empirical, and accurate method to establish the true  $T_{\text{eff}}$  scale of stars.

Typically  $F_{\text{bol}}$  is measured using flux-calibrated empirical templates (e.g., Pickles 1998) or models (Allard et al. 2012). Broadband photometry is used to inform which template or model is the best match to the star and used to derive the absolute flux calibration (for a more detailed description of this method see van Belle et al. 2008). Even when using the star’s true spectrum

instead of a template, the spectrum must be absolutely calibrated using photometry because of slit losses, atmospheric variability, etc.. Thus both methods are sensitive to errors in photometry, particularly errors common to entire photometric systems such as inaccuracies in the zero point and filter passband. Such errors could explain much of the systematic difference seen between  $F_{\text{bol}}$  values for the same stars when using different photometry (Boyajian et al. 2012; Mann et al. 2013b).

Most modern astronomical work can make use of precisely calibrated photometry from surveys such as the Sloan Digital Sky Survey (Stoughton et al. 2002; Abazajian et al. 2009) and the Two-Micron All-Sky Survey (2MASS, Skrutskie et al. 2006). However, long-baseline interferometry is currently limited to the largest and/or nearest stars, whose photometry is almost always saturated in such surveys. Instead, we must make use of older photometry, often from the General Catalog of Photometric Data<sup>5</sup> (GCPD, Mermilliod et al. 1997), which is a collection of photometry on  $> 200,000$  stars from  $> 2500$  papers. The GCPD contains more than 80 systems over a wide range of wavelengths, which makes it particularly useful for flux calibrating spectra and deriving spectral-energy distributions for bright stars. However, most of these photometric systems are calibrated no more precisely than 5% (see Bohlin et al. 2014, and references within).

Recent improvements in reduction techniques and instrumentation for long-baseline optical interferometry (e.g., Ireland et al. 2008; ten Brummelaar et al. 2012) have enabled the measurement of the stellar angular diameters ( $\theta$ ) to better than 2% for stars of sufficient brightness and angular size (e.g., Berger et al. 2006; Boyajian et al. 2013; Huber et al. 2013; von Braun et al. 2014).

<sup>1</sup> Harlan J. Smith Fellow, Department of Astronomy, The University of Texas at Austin, Austin, TX 78712, USA

<sup>2</sup> Visiting Researcher, Institute for Astrophysical Research, Boston University

<sup>3</sup> Lowell Observatory, 1400 W. Mars Hill Rd., Flagstaff, AZ, USA

<sup>4</sup> Max-Planck-Institute for Astronomy (MPIA), Konigstuhl 17, 69117 Heidelberg, Germany

<sup>5</sup> <http://obswww.unige.ch/gcpd/>

Errors of 1–2% in the angular diameter result in errors in  $T_{\text{eff}}$  of just 0.5–1% ( $\simeq 30$  K for a Sun-like star) ignoring errors in  $F_{\text{bol}}$ . In order to be limited by the error in  $\theta$  (which is typically the harder quantity to measure)  $F_{\text{bol}}$  must be measured with an error  $\lesssim 2\%$ . More importantly,  $F_{\text{bol}}$  values need to be free of systematic errors, which could conceivably arise from zero point and filter profile errors in the photometry, deviations in the shape of the spectrum, or inaccurate corrections for interstellar reddening.

When converting magnitudes into fluxes, a slightly erroneous filter profile (i.e., different from the true system profile) or red leak will result in color-terms (Bessell 1990; Bessell & Brett 1988). Specifically, flux derived from convolving the filter profile with the spectrum will differ from the flux calculated from corresponding photometry as a function of the color of the star. One can reverse-engineer the filter passband by calculating synthetic fluxes from precisely calibrated spectra, then comparing these values to the corresponding flux derived from the photometry of the same stars (e.g., Straizys 1996; Maíz Apellániz 2006). The filter profile can be adjusted until the difference between the synthetic and observed fluxes is a constant independent of the star’s color, and then the zero point adjusted until that constant is on average  $\simeq 0$ . This method is entirely empirical, and takes into account the full system throughput, but is limited by systematic errors in the spectral flux calibration.

In this paper we make use of several well-calibrated spectroscopic libraries to verify and derive revised filter bandpasses, zero points, and corresponding errors for photometry of bright stars (GCPD, Tycho-2, and *Hipparcos*). In Section 2 we describe our sample of spectroscopic libraries and in Section 3 we give a rundown of the photometric sample. In Section 4 we explain how we derive new filter bandpasses by forcing the synthetic and observed photometry to give consistent fluxes. In Section 5 we detail our revised properties for different photometric systems, compare our parameters to those in the literature, and estimate the error on our zero points. We conclude in Section 6 with a brief summary and highlight how our findings can significantly alter conclusions about  $F_{\text{bol}}$  values for cool stars.

## 2. SPECTROSCOPIC SAMPLE

A spectroscopic sample that is optimal for our purposes would include a large number ( $> 100$ ) of stars with photometry in the GCPD covering a wide range in  $B - V$  color, and contain spectra with significant wavelength coverage to include as many bands as possible. The MILES library (Sánchez-Blázquez et al. 2006; Falcón-Barroso et al. 2011) is one of the largest ( $\simeq 1000$  stars) and spans a wide range of  $B - V$  colors. However, MILES spectra cover only 3525–7000Å, which excludes sections of the bluest (e.g., Johnson  $U$ , Geneva  $U$ , Strömgren  $u$ ) and reddest (e.g., Cousins  $I$ ) optical filters. We resolve not to use MILES even for the passbands covered to maintain data homogeneity. Libraries like the Indo-U.S. Library (Valdes et al. 2004) have both wide wavelength coverage and a large number of stars, but the narrow slit, observing conditions, and joining of multiple observations with different gratings means that the flux calibration is unlikely to have sufficient precision and accuracy for our purposes.

For optical passbands we use the Next Generation Spectral Library (NGSL, Gregg et al. 2006; Heap & Linder 2007), which includes spectra of 374 stars spanning  $-0.3 < B - V < 1.8$ . NGSL spectra are taken with the Space Telescope Imaging Spectrograph (STIS) on the Hubble Space Telescope (HST) using three different gratings (G230LB, G430L, and G750L). This provides spectral coverage from 2000Å to 10000Å. The only optical filter in our sample (Section 3) not covered by NGSL spectra is Johnson  $I$ . Although the NGSL library contains fewer stars than MILES, the superior wavelength coverage is critical because it enables us to include far more filter systems in our analysis. Further, the relative flux calibration of HST STIS spectra is expected to be accurate to 0.5% (Bohlin et al. 2001; Bohlin & Gilliland 2004a,b), which is superior to what can currently be achieved from the ground.

For the NIR bands (Johnson  $JHKL$ ) we utilize the Infrared Telescope Facility (IRTF) spectral library (Cushing et al. 2005; Rayner et al. 2009), which includes 210 F, G, K, and M stars with wavelength coverage 8000–50,000Å. Only  $\simeq$  one third of these stars have  $JHK$  photometry in the GCPD, but this is better than comparable NIR catalogs, which tend to cover fainter stars that are less likely to be in the GCPD. The catalog also lacks the bluest stars ( $B - V < 0.15$ ), but goes significantly redder ( $B - V > 2$ ) than most spectroscopic catalogs.

Because only 49 stars in the IRTF library have NIR photometry in the GCPD we supplement the IRTF spectra with NIR spectra from ?, Mann et al. (2013b), and Gaidos et al. (2014). All of these stars are K and M dwarfs, which biases the sample toward redder  $B - V$  colors. However, the paucity of properly flux-calibrated NIR spectra makes this problem difficult to avoid. NIR spectra from these sources were taken with the same instrument and mode, and reduced in an identical manner to that of the IRTF library (Vacca et al. 2003; Cushing et al. 2004), except that the supplemental spectra cut off at 2.5μm while most stars in the IRTF library extend to 5μm.

We remove stars known to be highly variable ( $\gtrsim 0.1$  mag variability in  $V$ , Samus et al. 2004, 2010), stars lacking any photometry in the GCPD, those with an object of similar or greater brightness within 8'' (which will contaminate the photometry), and stars with questionable designations (e.g., the star labeled as GJ 15B in the NGSL catalog is probably GJ 15A based on the spectrum and HST pointing). This leaves 364 stars from the NGSL catalog, 49 stars from the IRTF library, and 59 stars from our supplemental spectra.

## 3. PHOTOMETRIC SYSTEMS

We focus our efforts on photometry from the GCPD because it is the most common source of photometry for bright interferometry stars. Many less commonly-used systems in the GCPD, such as Alexander (Jones et al. 1981) and Oja (Häggkvist & Oja 1970), lack photometry for stars in our spectroscopic sample. To determine the minimum number of spectra required we run our analysis (Section 4) on random subsets of the  $UBV$  filter sample. We find that if the subset contains  $\lesssim 40$  spectra (independent of how many photometric points there are per spectrum) the resulting filter profile is frequently ( $\gtrsim 30\%$  of the time) outside the range of profiles generated by our

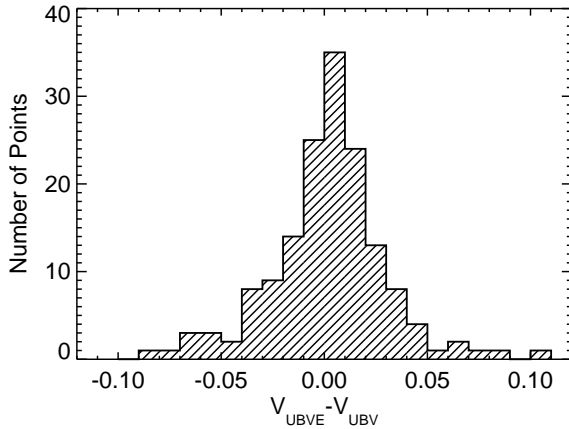


**Figure 1.** Comparison of  $V$  magnitudes from the GCPD  $UBVE$  and  $UBV$  systems. The median difference is 0.000, and the mean difference is 0.001 with a standard deviation of  $\simeq 0.02$ , which is consistent with measurement noise and/or stellar variability. Much of the photometry in the GCPD listed under different names are actually on the same system. See Section 3 for details.

analysis of the full set (see Section 5.2 for more details). We therefore require that to be included in our analysis a system/filter must have photometry for at least 40 stars in our spectroscopic sample and these  $\geq 40$  stars span at least 1 magnitude in  $B-V$  color. We exclude Johnson  $R$  and  $I$  from our tests. Johnson  $I$  is not fully covered by either of our spectral libraries, and Cousins  $R$  and  $I$  (which we do test) are more commonly used compared to their Johnson counterparts. We list all photometric systems tested in this paper in Table 1.

The GCPD differentiates between photometric systems even though they are in fact indistinguishable. The Straizys system (Kakaras et al. 1968) and Vilnius systems are identical;  $B$  and  $V$  from the Cape (GCPD name  $UcBV$ ) system are in the Johnson system; GCPD systems  $UBV$  and  $UBVE$  are indistinguishable (Figure 1); and (RI)C, Eggen, and  $UBVRI$  all contain Johnson  $U$ ,  $B$ , and/or  $V$  measurements in addition to their own unique system measurements. For our purposes we analyze systems with identical or nearly identical parameters together.

Initially we adopt the zero point and filter profile given in the GCPD (listed in Table 1). Many of these systems have been subsequently revised (e.g., Maíz Apellániz 2006; Bessell 2011; Bessell & Murphy 2012). However, our analysis only requires an approximate value for these as an initial guess. We compare our final filter profiles to updated literature values in Section 5.

In addition to the photometry listed in Table 1 we analyze photometry from *Hipparcos* (van Leeuwen & Fantino 2005; van Leeuwen 2007), and Tycho-2 (Høg et al. 2000). We download 2MASS photometry (for the NIR data), although we do not attempt to derive new zero points or filter profiles for 2MASS, as the calibration of our NIR data is not sufficiently precise to improve upon the calibration from Cohen et al. (2003). Rather, 2MASS data is only included to improve the absolute flux calibration of the NIR spectra. For *Hipparcos* and Tycho-2 photometry we use the initial zero points and system sensitivities from Bessell & Murphy (2012) and for 2MASS we use those from Cohen et al. (1992, 2003).

As noted by Bessell & Murphy (2012) and Casagrande & Vandenberg (2014), there is some confusion in the literature regarding photonic (photon-counting) versus energy response functions. Since the bands are generally normalized the difference is a factor of  $\int \lambda d\lambda$  (see Equations 2 and 3 below), which can be very significant for broadband photometry. For references that provide ambiguous information we assume they report photonic filter profiles, as we found this gave better agreement with our final results. We convert all photonic response curves to energy response functions (more appropriately called system sensitivity, which we denote as  $S_x$ ). The energy response is easier to use when calculating synthetic fluxes from flux-calibrated spectra (generally in energy units). For our derived filter profiles (Section 5, Appendix A) we report energy response functions.

Photometry for each star is downloaded from the GCPD using the python script *GCPD3*<sup>6</sup>. Photometry from *Hipparcos*, Tycho-2, and 2MASS (with errors) are downloaded using the IDL routine *QUERYVIZIER*<sup>7</sup>.

#### 4. ANALYSIS

Here we compare the literature photometry with the flux calibrated spectra and derive updated filter profiles, zero points, and photometric corrections.

##### 4.1. Comparing photometric fluxes to spectroscopic fluxes

The synthetic flux ( $f_{syn,x}$ ) is the flux in the sample spectrum, integrated over the filter profile, where the transmission of the filter is a wavelength dependent quantity, and is calculated using the formula:

$$f_{syn,x} = \frac{\int f_\lambda(\lambda) S_x(\lambda) d\lambda}{\int S_x(\lambda) d\lambda}, \quad (2)$$

where  $f_\lambda$  is the flux-calibrated spectrum<sup>8</sup> (e.g.,  $\text{erg cm}^{-2} \text{s}^{-1} \text{\AA}^{-1}$ ) as a function of wavelength ( $\lambda$ ).  $S_x(\lambda)$  is the system's *energy* sensitivity for the filter  $x$  (e.g.,  $U$ ,  $B$ ,  $V$ ), defined as:

$$S(\lambda) = QE(\lambda)\lambda, \quad (3)$$

where  $QE(\lambda)$  is the unit-less fractional transmission (i.e., photons detected/photons received). The combination of Equations 2 and 3 put us in accord with Equation A11 from Bessell & Murphy (2012) and Equation 3 from Bohlin et al. (2014). All synthetic fluxes are calculated using custom IDL routines, but we test to ensure consistency with the commonly used python tool *Pysynphot*.

Corresponding photometric fluxes from GCPD, *Hipparcos*, Tycho-2, and 2MASS photometry (denoted by  $f_{phot,x}$ ) are computed using the formula:

$$f_{phot,x} = f_{0,x} 10^{-0.4(m_x)} \quad (4)$$

where  $m_x$  is the magnitude and  $f_{0,x}$  is the zero point for band  $x$ . For this work we use flux units

<sup>6</sup> <https://github.com/awmann/GCPD3>

<sup>7</sup> <http://idlastro.gsfc.nasa.gov/ftp/pro/sockets/queryvizier.pro>

<sup>8</sup> The more appropriate term for  $f$  is radiative flux density or spectral irradiance, but for simplicity we use the more common astronomy term, flux or spectrum.

**Table 1**  
Photometric Systems and Initial Parameters

GCPD Name	Band	System Reference(s)	Center Å	$W_{\text{eff}}^{\text{a}}$ Å	$N_{\text{sp}}^{\text{b}}$	$N_{\text{ph}}^{\text{b}}$
<i>UcBV</i>	<i>U<sub>c</sub></i>	Arp (1958)	3948	376	56	71
	<i>U</i>	Johnson & Morgan (1951),	3517	665	299	1708
	<i>B</i>	Bessell (1990)	4454	1037	314	2168
	<i>V</i>		5523	909	315	2373
<i>uvby</i> (Strömgren)	<i>u</i>		3466	339	273	817
	<i>b</i>	Strömgren (1956),	4747	201	266	837
	<i>v</i>	Crawford & Mander (1966)	4073	200	266	818
	<i>y</i>		5479	256	267	882
Geneva	<i>U</i>		3467	479	269	267
	<i>B1</i>		4030	424	269	267
	<i>B</i>		4266	806	269	267
	<i>B2</i>	Golay (1972)	4486	445	269	267
	<i>V1</i>		5417	508	269	267
	<i>V</i>		5524	779	269	267
Vilnius	<i>G</i>		5821	485	269	267
	<i>U</i>		3450	395	180	387
	<i>P</i>		3740	276	180	387
	<i>X</i>		4054	254	181	392
	<i>Y</i>	Kakaras et al. (1968)	4665	288	180	392
	<i>Z</i>		5162	232	180	392
<i>WBVR</i>	<i>V</i>		5442	294	180	392
	<i>S</i>		6534	212	179	377
	<i>W</i>		3546	453	171	171
	<i>B</i>	Kornilov et al. (1991)	4400	881	171	171
DDO	<i>V</i>		5531	924	171	171
	<i>R</i>		7164	1312	171	171
	<i>m35</i>		3465	374	102	145
	<i>m38</i>		3825	327	122	185
	<i>m41</i>	McClure (1976)	4164	80	124	191
	<i>m42</i>		4255	71	124	191
(RI)C	<i>m45</i>		4520	73	124	191
	<i>m48</i>		4884	194	124	191
	<i>R</i>	Cousins (1976)	6507	1479	65	81
	<i>I</i>		7904	1042	67	84
(RI)Eggen	<i>R</i>	Eggen (1965)	6350	1200	113	126
	<i>I</i>		7900	900	113	94
<i>IJHKLMN</i>	<i>J</i>	Mendoza v. (1963),	12602	3268	87	154
	<i>H</i>	Bessell & Brett (1988)	16551	2607	89	144
	<i>K</i>		22094	5569	44	79
Tycho <sup>c</sup>	<i>B<sub>T</sub></i>	Bessell & Murphy (2012)	4213	693	342	342
	<i>V<sub>T</sub></i>		5345	1043	342	342
Hipparcos <sup>c</sup>	<i>H<sub>p</sub></i>	Bessell & Murphy (2012)	5593	2471	346	346

**Note.** — Details of the photometric sample can be found in Section 3.

<sup>a</sup> The effective width ( $W_{\text{eff}}$ ) is defined as:  $W_{\text{eff}} = \left( \int S_x(\lambda) d\lambda \right) / \max(S_x(\lambda))$ . This is essentially the equivalent width divided by the maximum throughput within the filter bandpass.

<sup>b</sup>  $N_{\text{ph}}$  is the number of photometric points included in our analysis,  $N_{\text{st}}$  is the number of spectra with measurements in that filter.  $N_{\text{ph}} \geq N_{\text{sp}}$  because many stars have more than one measurement in a given band.

<sup>c</sup> Tycho, and *Hipparcos* not in the GCPD, so we list their common name.

(erg cm<sup>-1</sup> s<sup>-2</sup> Å<sup>-1</sup>) rather than magnitudes when discussing zero points because they are more intuitive when discussing fractional differences (e.g., 30% is easier to imagine than 0.39 magnitudes) and because they are more practical for absolutely flux calibrating spectra. We report magnitudes where possible for reference.

In most cases, spectrophotometric libraries have precise *relative* flux calibrations (i.e., flux levels as a function of wavelength) but can still have significant absolute flux calibration errors (i.e., the whole spectrum is off by a constant). Bessell & Murphy (2012) solve this by renormalizing their spectra using precise *Hipparcos* ( $H_P$ ) magnitudes. Instead, we renormalize using all available photometry, which is also more resistant against outlier

photometry (e.g., taken during a flare) and enables us to include stars lacking  $H_P$  magnitudes. Specifically, after we compute synthetic and photometric fluxes we multiply each spectrum by a constant,  $C$ , which we define as:

$$C = \langle f_{\text{phot},x} / f_{\text{syn},x} \rangle, \quad (5)$$

where  $\langle \rangle$  denotes the median, which we calculate over all bands ( $x$ ) for a given star. This serves to absolutely flux calibrate each spectrum. The  $1\sigma$  error on  $C$  is assumed to be the standard deviation of  $f_{\text{phot},x} / f_{\text{syn},x}$  values after removing  $5\sigma$  outliers. Note that although we are calibrating the spectrum using uncorrected (and possibly erroneous) photometry, our process for fixing the photometric parameters is iterative and converges quickly (see

Section 4.2 for more details). We show two example calibrated spectra in Figure 2 with the photometric fluxes for comparison.

In theory it is possible to get a better  $C$  (and error estimate) using a robust weighted mean instead of a median. This is impractical because: a) measurement and zero point errors (and hence weights) for the GCPD photometry are not known, b) while Tycho-2 and *Hipparcos* report measurement errors, zero point errors are not known, and 3) a median does a better job at ignoring outlier photometry when there are only  $\simeq 5$  measurements.

We show the distribution of corrections ( $C$ ) applied to each of our libraries in Figure 3. The distribution similar to that derived for the NGSL library by Bessell & Murphy (2012), who renormalize their spectra using *Hipparcos* photometry alone. In general the corrections are small for the NGSL library, but there are a number of outliers with  $> 20\%$  corrections. Most of these outliers are also seen in the distribution of renormalizations from Bessell & Murphy (2012), although many they identify appear to be cut by our variability criterion (See Section 2). Corrections for the IRTF library often exceed 10%. Estimated errors on the normalization are also generally larger for the IRTF data ( $\sim 1\text{--}3\%$ ) than for the NGSL library ( $< 1\%$ ). This is because there are typically only 5–6 photometric points for a given star in the NIR (2MASS  $JHK_S$  and Johnson  $JHK$ ) while most of the NGSL stars have  $> 30$  photometric measurements, and because of lower precision flux calibration for the IRTF library.

Once the spectrum has been renormalized, we recalculate all synthetic fluxes following Equation 2. We then examine the ratio of photometric to synthetic flux ( $f_{phot,x}/f_{syn,x}$ ) as a function of  $B-V$ .  $B-V$  magnitudes for each star are computed Tycho-2  $B_T$  and  $V_T$  using the formula from Mamajek et al. (2002), where available. For stars lacking Tycho-2 magnitudes we use  $B-V$  colors from the GCPD. We use  $B-V$  as a measure of color because it is the only color index that is available for all stars in our spectroscopic sample.

We find significant discrepancies between synthetic and photometric flux as a function of  $B-V$  color (see Figure 4 for two examples). The shape and amplitude of the trend with  $B-V$  varies for each filter/system, but tends to be worse for filters with larger wavelength coverage (broader). Differences between photometric and spectroscopic fluxes of 10–20% are typical for broad filters and for the reddest and bluest stars. Both broad and narrow filters typically show systematic offsets ( $\simeq 5\text{--}10\%$ ) from a (median) flux ratio of unity.

The trends we see in  $f_{phot,x}/f_{syn,x}$  with  $B-V$  can be explained by errors in the filter profile. For example, an optical filter profile that is redder than the true system throughput will include extra flux from an M star because the SED of the M star is increasing with wavelength over the filter passband, but miss flux from an A star because the SED is decreasing. We illustrate a simple version of this effect in Figure 5. More complicated trends like that seen in Figure 4a are the consequence of multiple, overlapping issues with the filter profile. Errors in width, shape, and central wavelength of the filter passband combined with non-smooth spectra (e.g., a deep temperature sensitive feature somewhere in the passband) can give rise to such polynomial relations.

We note that most filters show trends significantly closer to linear than what we see with Johnson  $U$  shown in Figure 4.

Although the trends are large they are also relatively tight, specifically, the scatter around a polynomial fit to the data is small. An examination of the outlier points indicates that many of the stars have additional discrepant photometry in the same filter, suggesting stellar variability or erroneous measurements can explain much of the scatter. Although we screened for known variables and tighter binaries, many will be missed. For statistical purposes we do not remove any of these outlier points.

The disagreement between photometric and spectroscopic fluxes decreases if we adopt more recent system parameters from the literature. For example, if we use filter profiles and zero points from Bessell & Murphy (2012) for the Johnson  $U$ ,  $B$ , and  $V$  filters the  $B$  and  $V$  synthetic and photometry-based fluxes agree at the level of  $\simeq 2\text{--}6\%$ , compared to 10–15% when using the GCPD parameters. Small trends with  $B-V$  color are still present but only amount to 2–6% changes over 1.5 magnitudes in  $B-V$ . The improvement in  $U$  is much less significant (Figure 6). This is most likely because Bessell & Murphy (2012) make use of the MILES library, which does not cover all of the  $U$  band. Instead they have to interpolate past the end of their spectra, which introduces error.

#### 4.2. Deriving new system parameters

We derive a new passbands and zero points for each band using a Monte Carlo (MC):

- Adjust the filter profile’s *shift*, *skew*, and *broad*, which we define according to the following equations:

$$\lambda_{mod} = \lambda * shift \quad (6)$$

$$\lambda_{mod} = \lambda * ((\lambda - \lambda_{peak}) + 1)^{broad} \quad (7)$$

$$S_{mod}(\lambda) = S(\lambda) * \lambda^{skew}, \quad (8)$$

where  $\lambda_{mod}$  and  $S_{mod}$  are the wavelength and flux levels for the modified filter profile,  $\lambda_{peak}$  is the wavelength of maximum flux transmission. Figure 7 shows how each of these parameters changes the overall profile.

- Normalize filter profiles such that their maximum transmission is unity.
- Recalculate synthetic fluxes ( $f_{syn,x}$ ) for all stars from the calibrated spectra and the modified filter profile.
- Flag and remove points with  $f_{phot,x}/f_{syn,x}$  more than  $5\sigma$  outside a 20-point running robust mean.
- Calculate and apply a correction to zero point such that the median  $f_{phot,x}/f_{syn,x}$  is 1.
- Calculate the probability that  $B-V$  is correlated with  $f_{phot,x}/f_{syn,x}$  using a Spearman rank test (Spearman 1904).
- Compute the RMS scatter in  $f_{phot,x}/f_{syn,x}$ .

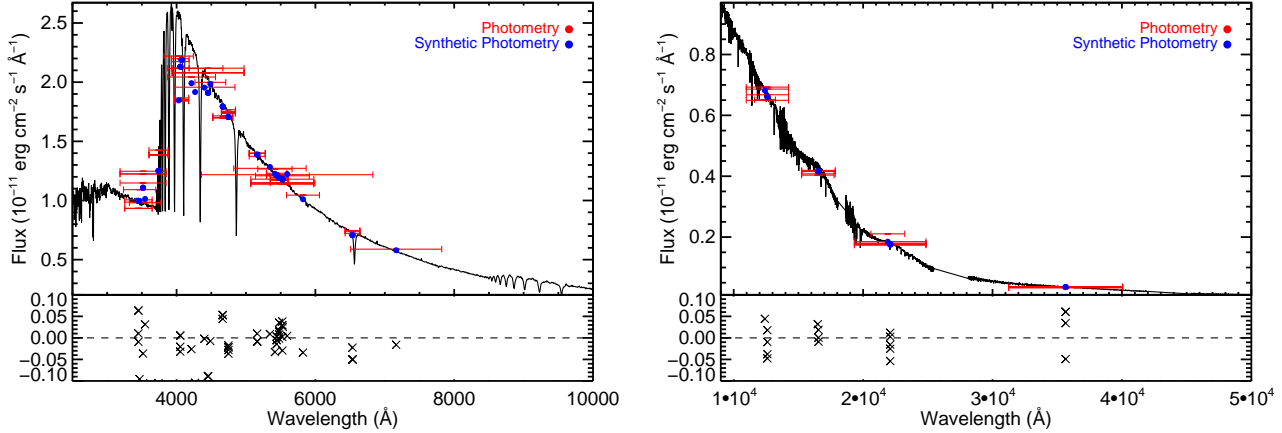


**Figure 2.** Demonstration of our flux calibration of the NGSL spectrum of the B9 dwarf HD 147550 (left) and the IRTF library spectrum of the M2 dwarf HD 95735 (right). Flux derived from photometry is shown in red with ‘error bars’ showing the approximate FWHM of the filter profile. Blue circles indicate the corresponding flux estimated from the spectrum (synthetic flux). Fractional residuals (synthetic - photometric)/synthetic are shown on the bottom panel of each figure. See Section 4.1 for more details.

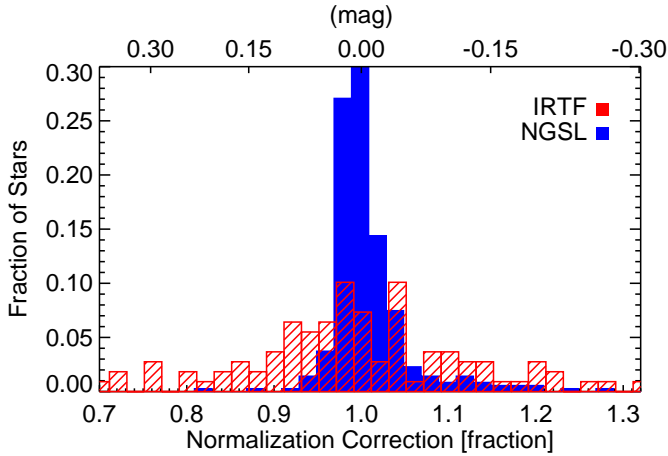


**Figure 3.** Distribution of normalizations applied to the NGSL and the IRTF library with the supplemental SpeX spectra. Five spectra have corrections  $> 30\%$  land outside the range of this plot, three of which are from our supplemental IRTF data. Changes in flux (as a fraction) are shown on the bottom X-axis with corrections in magnitudes on top for reference. See Section 4.1 for more details on our procedure to absolutely flux calibrate the spectra.

The above steps are repeated, each time adjusting the *shift*, *skew*, and/or *broad* parameters, which in turn alter the filter profile. *Shift* is varied from 0.9 to 1.1, *broad* from  $-2$  to  $2$ , and *skew* from  $-5$  to  $5$ , all in increments of  $0.01$ . The range of values for *shift*, *skew* and *broad* are conservatively large (by design); none of our final filter profiles are near the limits for any parameter. After the MC is complete, we adopt the filter parameters that yield a  $< 50\%$  probability of a correlation with  $B - V$  and the smallest scatter in  $f_{phot,x}/f_{syn,x}$ . We show illustrative examples of steps in the MC chain in Figure 8.

The Spearman rank test is best at identifying linear trends in the data. If there are significant non-linear trends in the data, a Spearman rank test might find a low probability of correlation even for highly correlated data. We remedy this by splitting the data into two subsets along the median  $B - V$  color and then recalculate the Spearman rank coefficient on each subset and for each MC step. We throw out profiles that show statistically

significant correlation in either subset. Examination of remaining  $f_{phot,x}/f_{syn,x}$  versus  $B - V$  color plots suggests this method is sufficient to remove obvious poor profiles.

The absolute flux calibration factors we apply to each spectrum (see Section 4.1, Figure 3) are based on uncorrected photometry. Although  $C$  (Equation 5) is calculated from the median of many points, the normalizations will still be slightly off due to errors in the filter parameters. To remedy this, we re-derive the absolute flux calibration constant for each library spectrum using the updated filter parameters. The changes are generally small, with a median normalization change of  $0.3\%$ , but the largest changes are  $>10\%$  (stars with few measurements or most measurements in the same filter), and show a trend with stellar color (the reddest and bluest stars change the most). After renormalizing the spectra with updated filter parameters we rerun the MC, deriving new filter profiles and zero points, this time with better-calibrated spectra. This process is repeated until changes in the derived zero points and filter profiles are negligible ( $< 0.1\%$ ). For most filters this happens after just 2–3 iterations, with the worst cases taking 5 iterations.

## 5. RESULTS

### 5.1. Updated Passbands and zero points

We list our final derived parameters for each system in Table 2. Zero points are given in  $\text{erg cm}^{-2} \text{s}^{-1} \text{\AA}^{-1}$ , but can be converted to magnitudes using the formula:

$$ZP_{mag} = -2.5 \log(ZP_{flux}) - 21.10. \quad (9)$$

Full normalized filter curves are given in the Appendix.

For Johnson *JHK* filters our derived passbands are indistinguishable from the original. Compared to other systems we examine, there is a paucity of measurements for *JHK* that overlap with our spectroscopic sample. Given this, and the larger errors associated with flux calibration of NIR data we decide to adopt the original filter profiles, but still adjust the zero points for these three filters.

In Figure 9 we show  $f_{phot,x}/f_{syn,x}$  as a function of  $B - V$  for two sample filters using our revised curves and zero points. Inspection of analogous plots for all filters and systems indicates that our profiles are removing

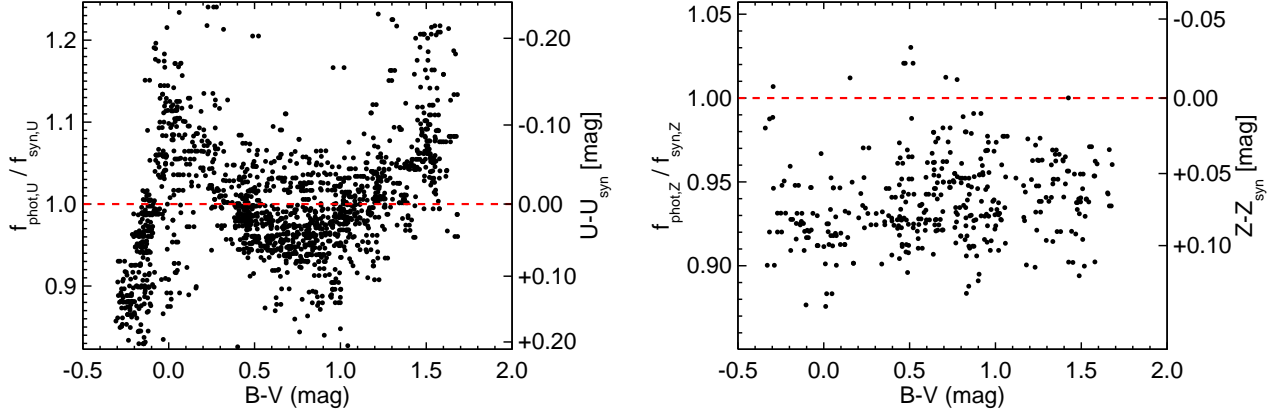


**Figure 4.** The ratio of flux from observed photometry ( $f_{phot}$ ) to that calculated from the spectra ( $f_{syn}$ ) as a function of  $B - V$  color for Johnson  $U$  (left) and Vilnius  $Z$  (right).  $B - V$  magnitudes are calculated from Tycho-2  $B_T$  and  $V_T$  where available, and from the GCPD elsewhere. The magnitude differences is shown on the right Y-axis for reference. Note that the Y-axis scales of the two plots are not the same. The red dashed line indicates agreement between photometric and spectroscopic fluxes. We have added an artificial scatter of 0.025 magnitudes in  $B - V$  to spread out overlapping points. See Section 4.1 for more information.

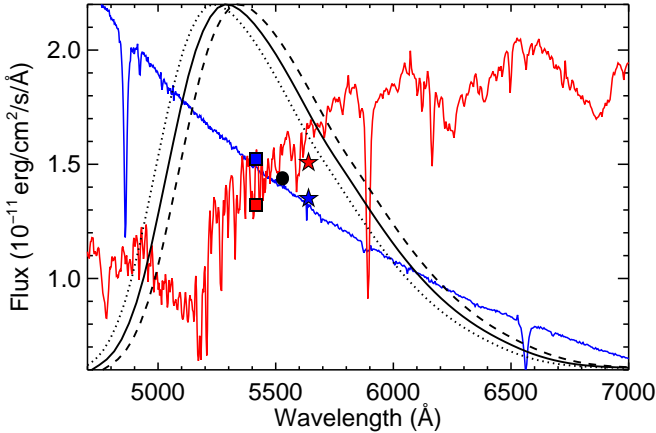


**Figure 5.** Example of how slightly inaccurate filter profiles create color-terms. We show the spectrum of the B6 star HD 174959 (blue) and the K7 star HD 201092 (red). These stars are selected because they have nearly identical  $V$  magnitudes. When we use the correct  $V$  filter profile (solid black line) the derived fluxes for both stars are nearly identical (black dot). If we shift the filter passband 1% redward (dashed line) the derived flux increases by  $\simeq 6\%$ , but decreases by  $\simeq 6\%$  for the B6 star (red and blue stars). The effect has a similar magnitude but opposite sign when we shift the filter blueward. More details can be found in Section 4.1

systematic trends in the data.

In Figure 10 we show a comparison of the input (original) zero points to those derived from our MC analysis. Of the 42 filters tested, 32 change by  $< 5\%$ , 6 change by 5–10%, and 4 change by  $> 10\%$ . Input zero points are meant as an initial guess for the MC, and are not necessarily the best available. Thus we also compare to the more recent analysis of Bessell & Murphy (2012) for Johnson  $UBV$ , Cousins  $RI$ , *Hipparcos*, and Tycho-2 photometry. Our zero points are within 2% of those from Bessell & Murphy (2012), with the exception of the Johnson  $U$  filter, for which we disagree by 5%. We suspect the difference is due to their use of the MILES library, which does not cover the full  $U$  band.

In Figures 11, 12, and 13 we compare our derived filter profiles to those from Bessell (2011) and Bessell &

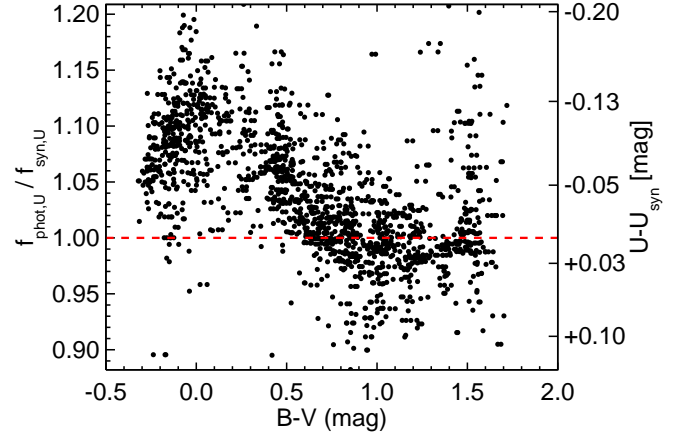


**Figure 6.** Similar to Figure 4 for the Johnson  $U$  band, but using the zero points and passbands are taken from Bessell & Murphy (2012). This is an improvement over the older system parameters but a significant trend is still seen. Note that the Y-axis scale is similar but not identical to that in Figure 4.

Murphy (2012). The differences appear relatively small, but small differences can have a big impact for the bluest and reddest stars (see Figures 4 and 6). Note that zero point and filter profile changes are also correlated. If we adopt the input filter profiles we derive zero points which are generally closer to the originals, but this reintroduces color-terms.

## 5.2. Understanding Errors

One important aspect of our analysis is to come up with an estimate for the error on the zero points. A simple method would be to calculate the standard error on the ratios of observed to synthetic fluxes ( $f_{phot,x} / f_{syn,x}$ ). Because most bands have  $\gg 100$  points and the standard deviation of  $f_{phot,x} / f_{syn,x}$  within a given filter tends to be small (1–3%), this method would suggest zero point errors  $\lesssim 0.2\%$ . This is unrealistically small because our analysis is dominated by systematic errors. In particular the largest source of error is errors in the spectrophotometric calibration of the NGSL or IRTF spectra.

**Table 2**  
Final zero points and Passband Parameters

Name	Band	zero point $10^{-9} \text{ erg cm}^{-1} \text{ s}^{-2} \text{ Å}^{-1}$	$\pm$	Center Å	$W_{\text{eff}}$
Cape	$U_C$	23.25	0.14	3925	999
Johnson	U	4.264	0.022	3620	1380
	B	6.459	0.032	4412	1816
	V	3.735	0.019	5529	1129
	J	0.310	0.003	12603	2095
	H	0.113	0.001	16552	1362
	K	0.0400	0.0005	22094	2142
Stromgren	u	11.72	0.06	3485	950
	b	5.974	0.030	4671	338
	v	8.691	0.044	4125	513
	y	3.778	0.019	5474	596
Geneva	U	5.612	0.029	3453	1404
	B1	6.676	0.034	4031	861
	B	2.838	0.014	4230	1523
	B2	10.76	0.05	4448	597
	V1	7.460	0.038	5379	788
	V	3.728	0.019	5495	1220
Vilnius	G	9.462	0.048	5785	543
	U	18.75	0.10	3478	884
	P	14.30	0.08	3750	418
	X	11.28	0.06	4061	584
	Y	6.792	0.035	4697	725
	Z	4.583	0.023	5204	244
WBVR	V	3.772	0.019	5464	584
	S	1.863	0.010	6520	271
	W	3.523	0.018	3554	963
	B	6.619	0.034	4382	1495
DDO	V	3.730	0.019	5519	1394
	R	1.698	0.009	7166	1360
	m35	13.02	0.07	3521	1015
	m38	6.867	0.037	3864	709
	m41	21.16	0.11	4182	211
	m42	19.97	0.10	4257	145
Cousins	m45	13.15	0.07	4512	141
	m48	4.966	0.025	4912	437
	R	2.215	0.012	6615	1877
Eggen	I	1.163	0.007	8047	1604
	R	2.293	0.016	6989	2831
Tycho	I	1.337	0.011	8492	1330
	Bt	6.798	0.034	4220	1455
	Vt	4.029	0.020	5350	1665
Hipparcos	Hp	3.926	0.020	5586	2569

**Note.** — Zero points are all derived from our MC analysis (see Section 4). Errors are calculated from estimates of systematic errors in the flux calibration of our spectra and the standard error (see Section 5.2). Full filter profiles are given in the Appendix.

Flux calibration better than 1% in the NIR is extraordinarily difficult because time-dependent changes in the sky (seeing, transmission, etc.) create wavelength-dependent flux losses that vary between target and standard observations. Cushing et al. (2005) and Rayner et al. (2009) mitigate for this by observing at the parallactic angle. By absolutely calibrating the library to 2MASS and comparing the residuals, Rayner et al. (2009) estimate that the IRTF library has spectral slopes accurate to 1–3% percent, although our own analysis suggests it is  $\simeq 1\%$ , and much of the variation actually arises because of larger errors in 2MASS photometry for the brightest stars (non-linear part of the detector or saturation). Differences between 2MASS and the IRTF spectra are consistent with random errors, but we cannot rule out (systematic) slope errors of 1%. To be conservative we add 1% errors in quadrature with the standard errors calculated for zero points on *JHK* photometry.

Space-based spectra should be able to achieve ex-

tremely accurate relative flux calibrations, since the major source of error for ground-based observations is removal of time-dependent noise from the sky (Young et al. 1991; Mann et al. 2011). However, the instrument and telescope can also introduce slope changes. In fact, an earlier version of the NGSL had significant errors in the spectral shape due to imperfect centering of the target on the slit. This was later calibrated out in post-processing, but highlights the difficulties in precisely flux calibrating spectra.

To test the level of noise expected from shape errors we compare NGSL spectra with well flux-calibrated ground-based spectra from Mann et al. (2013b) for 10 overlapping stars (see Figure 14 for an example). Slope differences are  $< 2\%$  in all cases, and on average are 0.9%. Mann et al. (2013b) report slope errors of 0.5–1% in their spectra based on repeat observations. This suggests most of the difference between the ground- and space-based spectra can be explained by errors in the ground-based

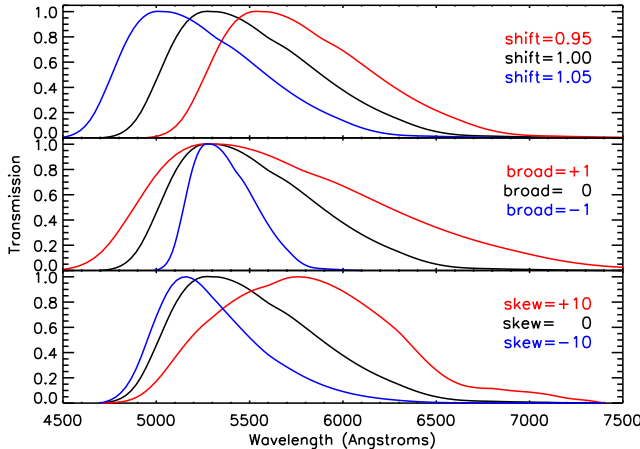


**Figure 7.** The effects of Equations (5)-(7) on the filter profile. *Shift* moves the central wavelength, *broad* adjusts how narrow or broad the profile is, and *skew* changes relative transmission between the blue and red end of the profile. Relatively large values of each parameter are used for this Figure to make the effect more clear.

data. With this small comparison sample we cannot rule out slope errors as large as 0.5%, so we conservatively add this to the standard errors on the zero points for all optical photometry. Final zero point errors are listed in Table 2 for all systems included in our analysis.

For any given filter our analysis produces a large number of acceptable filter profiles, i.e. profiles which have no statistically significant color terms and an RMS in  $f_{phot,x}/f_{syn,x}$  within a factor of two of the smallest RMS (we adopt the smallest RMS as the true filter). In Figure 15 we show an example distribution of all acceptable filter profiles that comes out of our MC analysis. For all filters the distribution is similarly tight, which suggests that the adopted profiles are fairly reliable and that we are getting close to the real system parameters. This also suggests that errors on our derived filter profiles are relatively small.

## 6. SUMMARY AND DISCUSSION

In our effort to improve measurements of  $F_{bol}$  and, by extension  $T_{eff}$  and/or  $R_*$ , we tested the zero points and passbands for 42 different filters across a range of photometric systems. To this end we took advantage of the precise relative flux calibration of the NGSL and IRTF spectral libraries. By comparing flux calculated from the photometry to the corresponding flux in the spectrum we showed that errors in zero points and filter passbands can lead to flux errors of  $> 25\%$  for the bluest and reddest stars.

To derive new passbands and zero points, we ran an MC analysis on each of the 42 filters in our sample. The MC found the filter parameters that produce the best agreement between spectroscopic and photometric fluxes free of correlations with the color of the star. For most bands the changes were relatively small (e.g.,  $< 5\%$  in zero points), but some changed by  $> 10\%$ . Changes in filter profiles were also generally small, but still had a very significant effect on stars with extreme colors, and hence are important to avoiding systematic errors.

We estimated errors in our zero points by considering possible shape (relative flux calibration) errors in the

NGSL and IRTF spectra. Based on a comparison to spectra from other sources, we estimated that the relative flux calibration of the NGSL library is good to  $\lesssim 0.5\%$ , although this may be a conservative estimate. For the IRTF spectra, the flux calibration is worse because of the complications involved in flux calibration NIR spectra from the ground. We expect that zero points for NIR filters are still good to  $\simeq 1\%$  for most bands.

We also have estimated errors on the filter profiles by considering the range of reasonable filter profiles that come out of our MC analysis (Figure 15). We report these errors alongside our derived filter profiles in the Appendix. However, readers are cautioned that these errors are highly correlated. For example, if we adopt transmission values lower than the best-fit value for the red end of the filter, then it's likely we will have to reduce the throughput in the blue in order to avoid introducing a color term.

Our analysis has assumed that the true filter profile is a simple correction to the original profile. More complicated changes are more difficult to take into account because it makes parameter space too wide for the number of data points. For example, red leaks, which are common for blue filters, can easily give rise to color terms like those seen in this paper. However, most CCDs optimized for blue filters have low quantum efficiency in the red, and hence are only mildly affected by red leaks. Given that we are able to derive filter profiles free of color terms even for photometry taken from different sources, using different detectors and optical systems suggests that few, if any of these filters are subject to very significant red leaks. Future analysis with additional spectra will enable us to search using more complicated filter profiles and confirm this suggestion empirically.

The presented revisions (see Table 2) are derived based on data in our spectroscopic sample that span the range  $-0.4 \lesssim B - V \lesssim 1.7$ . Consequently, we caution the reader that there may be color-terms in the filter profiles that only become apparent at more extreme red and blue colors.

We note that our derived system sensitivities are not necessarily the true profile. It is certainly possible that a system sensitivity could produce no color terms and still not match the original standards, although this raises the issue of whether it is possible to define a true system in an absolute sense. Original system definitions are rarely determined with the precision we can achieve today. It is unlikely that CCDs and filters installed are perfect clones of the original system, and even if they were, filters/instruments are often changed and observations are corrected using imperfect transformations to put data back onto the standard systems. This data amalgamation makes it difficult to define a single system sensitivity that describes all the photometry. However, narrow range of system profiles that comes out of our MC analysis is promising, and suggestive that even if our parameters do not match the original system they are useful and accurate for calculating synthetic photometry and fluxes.

Future efforts to calibrate NIR photometry will require spectra with better spectrophotometric calibration. The X-Shooter library (Chen et al. 2011) offers a special advantage because it is build from optical and NIR spectra taken simultaneously. In this case optical photometry

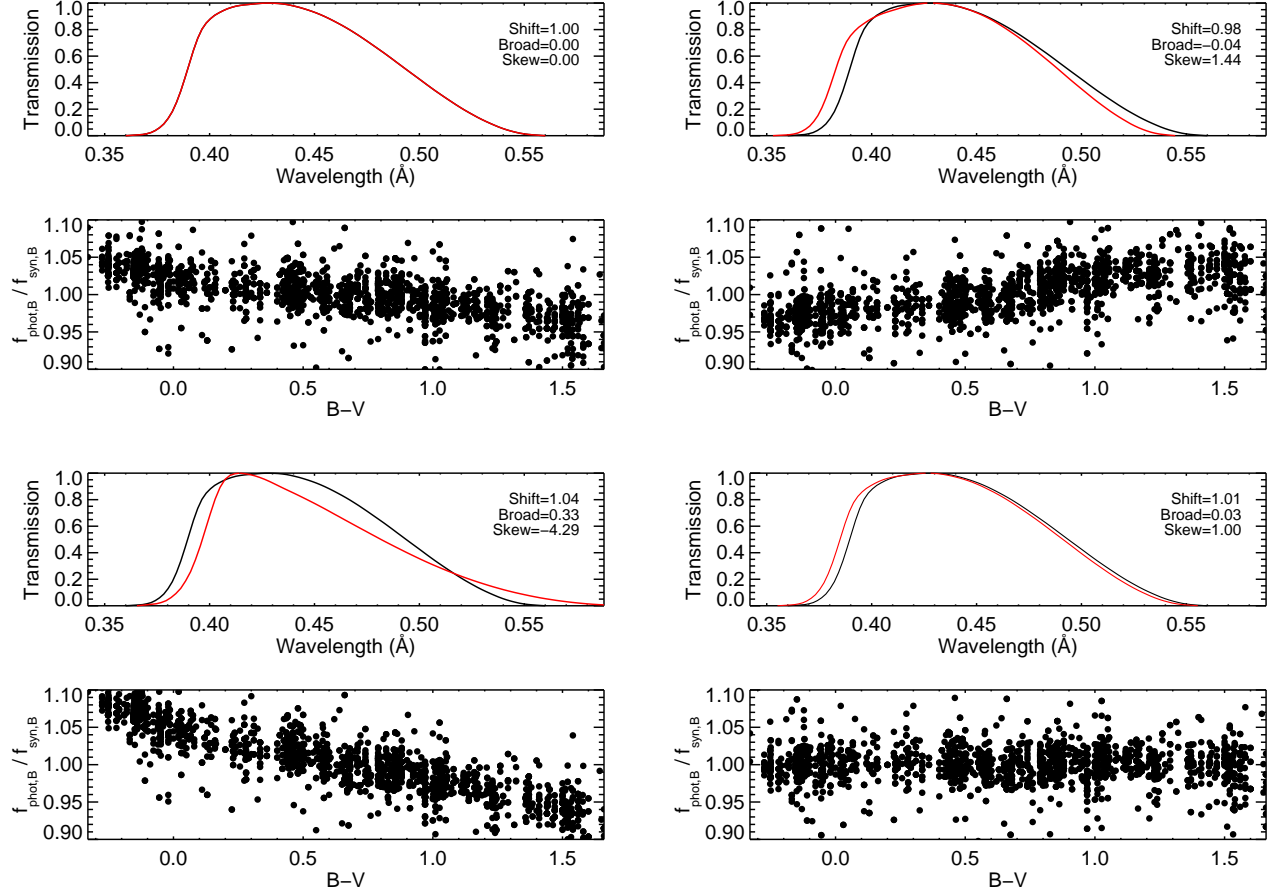


**Figure 8.** Four example steps in the MC chain for the Johnson  $B$  filter. The top of each pane shows the filter profile adopted by that step in red, with the initial input profile in black, along with the *skew*, *shift*, and *broad* parameters in the legend. The bottom of each pane is analogous to Figures 4 and 6. Each pane represents a different step in the MC, with the top-left showing the initial value, and the bottom right showing the final result, and the other top right and bottom left displaying representative spots along the chain. Axis ranges are identical in all plots. Our MC procedure is described in Section 4.2.

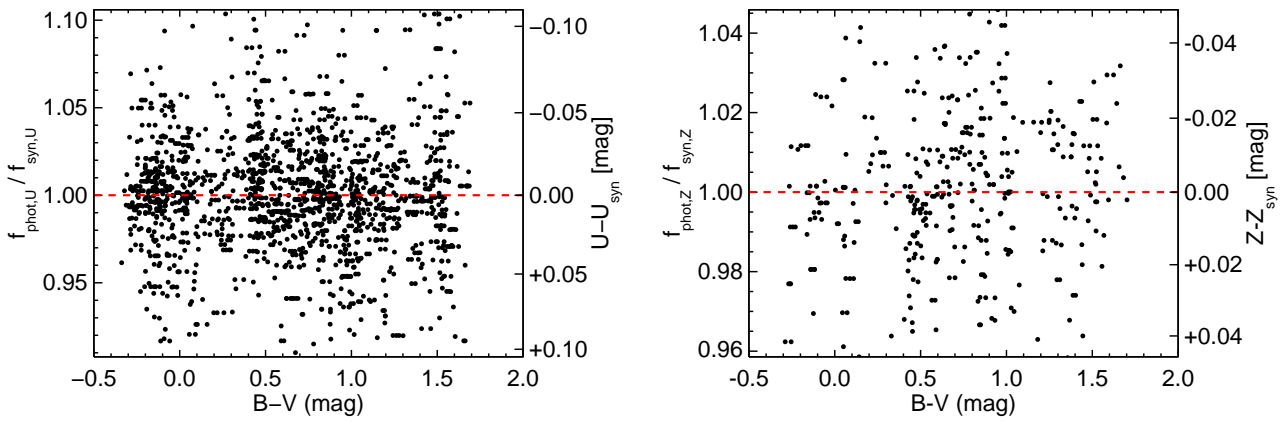


**Figure 9.** Similar to Figure 4, but using our revised filter profiles and zero points. Note that the Y-axis scales of the two plots are not the same, nor are they the same as those in Figure 4. For  $Z$  and  $U$  respectively there are 3 and 8 outlier points outside the scale of the Figures. These are most likely variable stars, erroneous measurements, or measurements assigned to the wrong star as the scatter in repeat measurements with the same filter on the same star is typically only 0.02–0.04 mags. The red dashed line indicates agreement between photometric and spectroscopic fluxes. Consult Section 5.1 for more information.

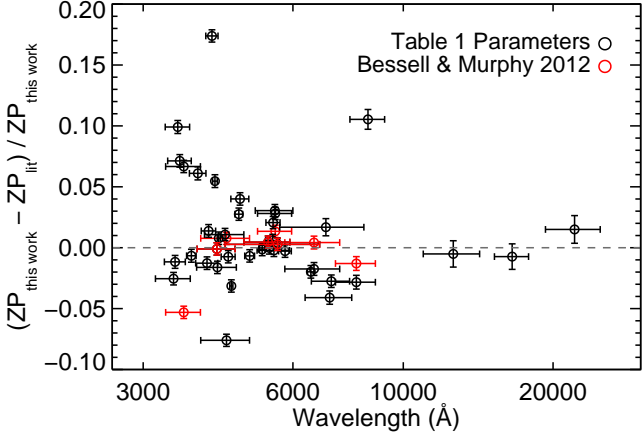


**Figure 10.** Fractional difference between zero points derived in this work and those from Table 1. Horizontal error bars indicate the  $W_{\text{eff}}$  for the given filter. Vertical error bars show the estimated error in our own zero points. While many filters change by  $< 5\%$ , five change by more than  $10\%$ , including three off the scale of the Figure. Zero points from Bessell & Murphy (2012) are shown (in red) for reference. See Section 5 for more details.

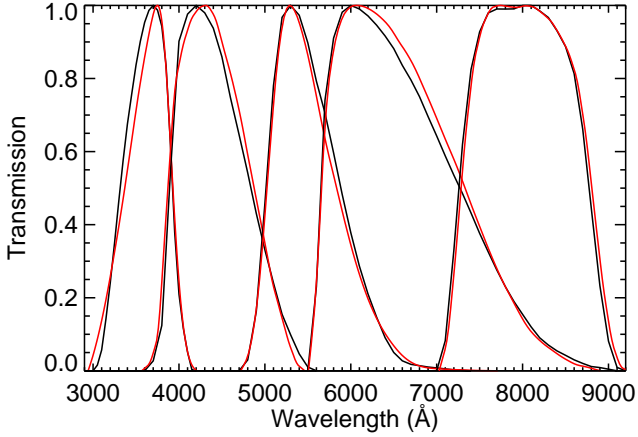


**Figure 11.** Filter response curves derived from our analysis (red) compared to those from Bessell & Murphy (2012) for Johnson  $UVW$  and Cousins  $RI$  filters. Note all filters are shown as energy response curves.

can be used to absolutely flux calibrate the spectrum, and then the NIR region can be used to independently test the NIR photometry. Unfortunately, the currently available version of the X-shooter library contains only optical data. Another advance will come with the expansion of the NGSL library (HST approved program ID 13776). This is expected to widen the color of the sample and provide an opportunity to revise/test the spectrophotometric calibration.

One of the primary motivations of this study was to significantly improve on the precision and accuracy of derived bolometric fluxes for stars observed with long-baseline optical interferometry. The shifts in filter profiles are especially important for this, because color terms will lead to systematic differences in the absolute photometry. This will correspondingly shift the absolute flux calibration, and hence, the derived  $F_{\text{bol}}$  and  $T_{\text{eff}}$  for any given star.

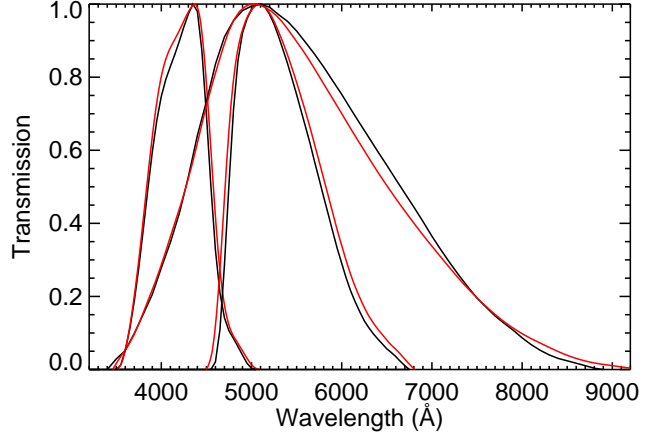


**Figure 12.** Same as Figure 11 but for Hipparcos and Tycho-2 passbands. The broadest passband is the Hipparcos filter.

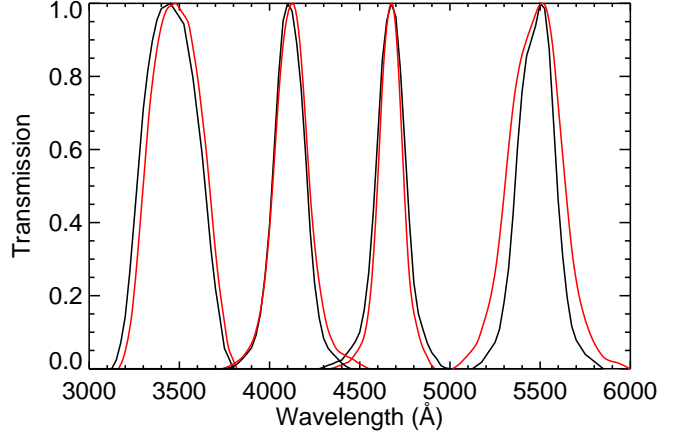


**Figure 13.** Same as Figure 11 but for Strömgren ( $ubvy$ ) passbands from Bessell (2011).

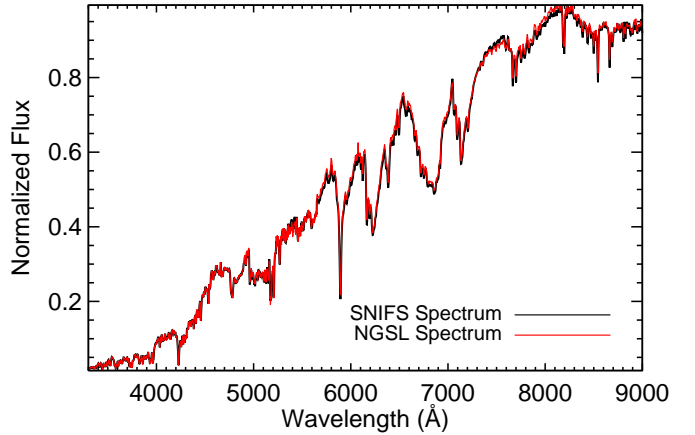


**Figure 14.** Ground-based optical spectrum (black) taken from Mann et al. (2013b) compared to a STIS spectrum (red) from NGSL of the star HD 1326 (GJ 15A). Both spectra have been normalized to their peak value. The differences in slope are  $\simeq 1\%$ , which is consistent with expected errors from SNIFS. See Section 5.2 for more information.

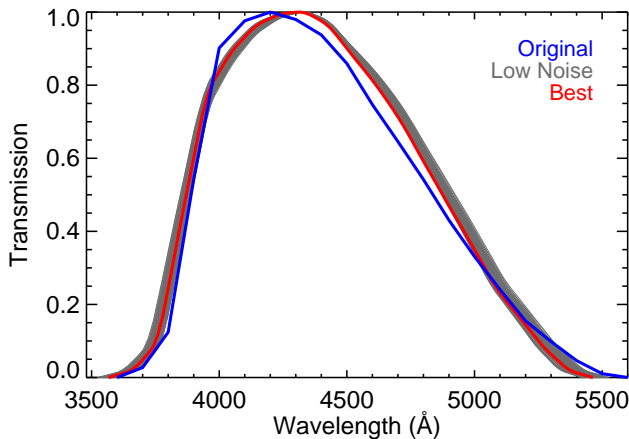


**Figure 15.** Filter profile for the Johnson  $B$  filter with original denoted in blue, and the best (adopted) profile shown in red. All filter profiles that show no correlation between  $f_{phot,x}/f_{syn,x}$  and  $B - V$  and have an RMS in  $f_{phot,x}/f_{syn,x}$  less than double the minimum RMS (ones we consider acceptable solutions) that came out of our MC analysis are shown in grey. The original filter has been converted to energy response (as opposed to photon counting) for consistency with our analysis. See Section 5.2 for more information.

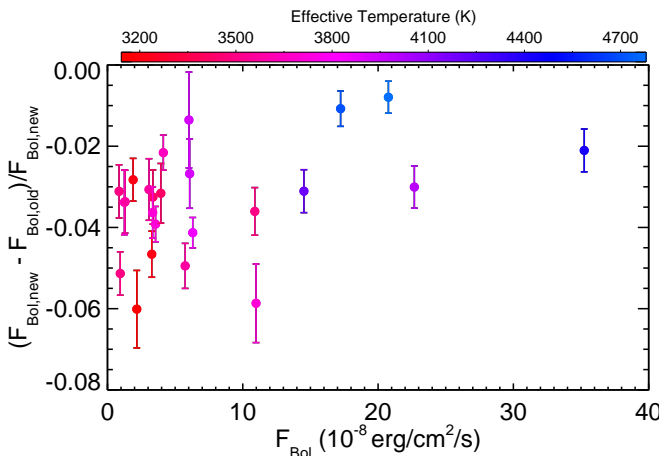


**Figure 16.** Values of  $F_{bol}$  calculated using updated parameters from this work (new) compared to those calculated using the original input parameters (old). Errors are calculated from the scatter in the normalization and measurement errors in the spectrum.

We highlight this point by recalculating  $F_{bol}$  for the K and M dwarfs from Boyajian et al. (2012) and Mann et al. (2013b), first using the original system parameters and then using the updated parameters from this work. We follow the same procedure to flux calibrate the spectra, i.e., use the median correction from all available photometry. As in Mann et al. (2013b), we extrapolate beyond the edges of the spectrum using a Rayleigh-Jeans law or Wien's approximation for the red and blue end, respectively. The  $F_{bol}$  is then calculated from the numerical integral of the entire spectrum. In Figure 16 we show the comparison of  $F_{bol}$  using old and new photometric system parameters. There is a clear systematic offset caused by the differences in absolute flux calibrations. This amounts to a median offset of 3%, which is statistically significant for most stars, and is highly significant if

we consider the full sample. Further, the offset is larger for the coolest (reddest) stars (3–7%), emphasizing the importance of accurate photometric system parameters to reducing systematic errors.

The authors thank the referee, Ralph Bohlin, for his extremely quick and useful review of this work. We also thank Megan Ansdell, Eric Gaidos, and Chao-Ling Hung for their useful comments on this manuscript. We give additional thanks to Simon Murphy, Tabetha Boyajian, and Gerard van Belle for their useful discussions at Cool Stars 18. This work was supported by the Harlan J. Smith Fellowship from the University of Texas at Austin to AWM.

This research has made use of the SIMBAD database, operated at CDS, Strasbourg, France. This work is based on observations made with the NASA/ESA Hubble Space Telescope, obtained at the Space Telescope Science Institute, which is operated by the Association of Universities for Research in Astronomy, Inc., under NASA contract NAS 5-26555. These observations are associated with GO program 11652.

Facility: IRTF

## REFERENCES

- Abazajian, K. N., Adelman-McCarthy, J. K., Agüeros, M. A., et al. 2009, [ApJS, 182, 543](#)
- Allard, F., Homeier, D., Freytag, B., & Sharp, C. M. 2012, in [EAS Publications Series, Vol. 57, EAS Publications Series, 3](#)
- Arp, H. C. 1958, [AJ, 63, 118](#)
- Berger, D. H., Gies, D. R., McAlister, H. A., et al. 2006, [ApJ, 644, 475](#)
- Bessell, M., & Murphy, S. 2012, [PASP, 124, 140](#)
- Bessell, M. S. 1990, [PASP, 102, 1181](#)
- . 2011, [PASP, 123, 1442](#)
- Bessell, M. S., & Brett, J. M. 1988, [PASP, 100, 1134](#)
- Blackwell, D. E., & Shallis, M. J. 1977, [MNRAS, 180, 177](#)
- Bohlin, R. C., Dickinson, M. E., & Calzetti, D. 2001, [AJ, 122, 2118](#)
- Bohlin, R. C., & Gilliland, R. L. 2004a, [AJ, 128, 3053](#)
- . 2004b, [AJ, 127, 3508](#)
- Bohlin, R. C., Gordon, K. D., & Tremblay, P.-E. 2014, [PASP, 126, 711](#)
- Boyajian, T. S., von Braun, K., van Belle, G., et al. 2012, [ApJ, 757, 112](#)
- . 2013, [ApJ, 771, 40](#)
- Casagrande, L., Portinari, L., & Flynn, C. 2006, [MNRAS, 373, 13](#)
- Casagrande, L., Ramírez, I., Meléndez, J., Bessell, M., & Asplund, M. 2010, [A&A, 512, A54](#)
- Casagrande, L., & Vandenberg, D. A. 2014, [MNRAS, 444, 392](#)
- Chen, Y., Trager, S., Peletier, R., & Lançon, A. 2011, [Journal of Physics Conference Series, 328, 012023](#)
- Cohen, M., Walker, R. G., Barlow, M. J., & Deacon, J. R. 1992, [AJ, 104, 1650](#)
- Cohen, M., Wheaton, W. A., & Megeath, S. T. 2003, [AJ, 126, 1090](#)
- Cousins, A. W. J. 1976, [MmRAS, 81, 25](#)
- Crawford, D. L., & Mander, J. 1966, [AJ, 71, 114](#)
- Cushing, M. C., Rayner, J. T., & Vacca, W. D. 2005, [ApJ, 623, 1115](#)
- Cushing, M. C., Vacca, W. D., & Rayner, J. T. 2004, [PASP, 116, 362](#)
- Eggen, O. J. 1965, [AJ, 70, 19](#)
- Falcón-Barroso, J., Sánchez-Blázquez, P., Vazdekis, A., et al. 2011, [A&A, 532, A95](#)
- Gaidos, E., Mann, A. W., Lépine, S., et al. 2014, [MNRAS, 443, 2561](#)
- Golay, M. 1972, [Vistas in Astronomy, 14, 13](#)

- Gregg, M. D., Silva, D., Rayner, J., et al. 2006, in The 2005 HST Calibration Workshop: Hubble After the Transition to Two-Gyro Mode, ed. A. M. Koekemoer, P. Goudfrooij, & L. L. Dressel, 209
- Häggkvist, L., & Oja, T. 1970, *A&AS*, 1, 199
- Heap, S. R., & Lindler, D. J. 2007, in Astronomical Society of the Pacific Conference Series, Vol. 374, From Stars to Galaxies: Building the Pieces to Build Up the Universe, ed. A. Vallenari, R. Tantalo, L. Portinari, & A. Moretti, 409
- Høg, E., Fabricius, C., Makarov, V. V., et al. 2000, *A&A*, 355, L27
- Huber, D., Chaplin, W. J., Christensen-Dalsgaard, J., et al. 2013, *ApJ*, 767, 127
- Ireland, M. J., Mérand, A., ten Brummelaar, T. A., et al. 2008, in Society of Photo-Optical Instrumentation Engineers (SPIE) Conference Series, Vol. 7013, Society of Photo-Optical Instrumentation Engineers (SPIE) Conference Series
- Johnson, H. L., & Morgan, W. W. 1951, *ApJ*, 114, 522
- Jones, D. H. P., Sinclair, J. E., & Alexander, J. B. 1981, *MNRAS*, 194, 403
- Kakaras, G., Straizys, V., Sudzius, J., & Zdanavicius, K. 1968, Vilnius Astronomijos Observatorijos Biuletenis, 22, 3
- Kornilov, V. G., Volkov, I. M., Zakharov, A. I., et al. 1991, Trudy Gosudarstvennogo Astronomicheskogo Instituta, 63, 1
- Maíz Apellániz, J. 2006, *AJ*, 131, 1184
- Mamajek, E. E., Meyer, M. R., & Liebert, J. 2002, *AJ*, 124, 1670
- Mann, A. W., Brewer, J. M., Gaidos, E., Lépine, S., & Hilton, E. J. 2013a, *ApJ*, 145, 52
- Mann, A. W., Gaidos, E., & Aldering, G. 2011, *PASP*, 123, 1273
- Mann, A. W., Gaidos, E., & Ansdel, M. 2013b, *ApJ*, 779, 188
- McClure, R. D. 1976, *AJ*, 81, 182
- Mendoza v., E. E. 1963, Boletín de los Observatorios Tonantzintla y Tacubaya, 3, 137
- Mermilliod, J.-C., Mermilliod, M., & Hauck, B. 1997, *A&AS*, 124, 349
- Pickles, A. J. 1998, *PASP*, 110, 863
- Rayner, J. T., Cushing, M. C., & Vacca, W. D. 2009, *ApJS*, 185, 289
- Samus, N. N., Durlevich, O. V., & et al. 2004, VizieR Online Data Catalog, 2250, 0
- Samus, N. N., Kazarovets, E. V., Kireeva, N. N., Pastukhova, E. N., & Durlevich, O. V. 2010, Odessa Astronomical Publications, 23, 102
- Sánchez-Blázquez, P., Gorgas, J., Cardiel, N., & González, J. J. 2006, *A&A*, 457, 787
- Skrutskie, M. F., Cutri, R. M., Stiening, R., et al. 2006, *AJ*, 131, 1163
- Sneden, C. A. 1973, PhD thesis, the University of Texas at Austin
- Sousa, S. G., Alapini, A., Israeli, G., & Santos, N. C. 2010, *A&A*, 512, A13
- Sousa, S. G., Santos, N. C., Israeli, G., Mayor, M., & Udry, S. 2011, *A&A*, 533, A141
- Spearman, C. 1904, American Journal of Psychology, 15, 88
- Stoughton, C., Lupton, R. H., Bernardi, M., et al. 2002, *AJ*, 123, 485
- Straizys, V. 1996, Baltic Astronomy, 5, 459
- Strömgren, B. 1956, *Vistas in Astronomy*, 2, 1336
- ten Brummelaar, T. A., Sturmann, L., Sturmann, J., et al. 2012, in Society of Photo-Optical Instrumentation Engineers (SPIE) Conference Series, Vol. 8447, Society of Photo-Optical Instrumentation Engineers (SPIE) Conference Series
- Vacca, W. D., Cushing, M. C., & Rayner, J. T. 2003, *PASP*, 115, 389
- Valdes, F., Gupta, R., Rose, J. A., Singh, H. P., & Bell, D. J. 2004, *ApJS*, 152, 251
- Valenti, J. A., & Piskunov, N. 1996, *A&AS*, 118, 595
- van Belle, G. T., van Belle, G., Creech-Eakman, M. J., et al. 2008, *ApJS*, 176, 276
- van Leeuwen, F. 2007, *A&A*, 474, 653
- van Leeuwen, F., & Fantino, E. 2005, *A&A*, 439, 791
- von Braun, K., Boyajian, T. S., van Belle, G. T., et al. 2014, *MNRAS*, 438, 2413
- Young, A. T., Genet, R. M., Boyd, L. J., et al. 1991, *PASP*, 103, 221

## APPENDIX

Here we provide our final filter profiles. Electronic versions are available with this submission.

**Table 3**  
Energy Response Functions,  $S_x(\lambda)$ , for Johnson

$\lambda$ Å	<i>U</i>		<i>B</i>		<i>V</i>		<i>R</i>	
	Trans	$\lambda$ Å	Trans	$\lambda$ Å	Trans	$\lambda$ Å	Trans	$\lambda$ Å
2942.0	0.000	3566.0	0.000	4718.2	0.000	5945.3	0.000	
2959.1	0.012	3591.6	0.005	4758.6	0.017	5990.7	0.028	
2976.2	0.024	3617.3	0.010	4799.1	0.041	6036.0	0.061	
2993.3	0.037	3642.9	0.016	4839.5	0.078	6081.3	0.107	
3010.4	0.051	3668.6	0.027	4880.0	0.134	6126.7	0.179	
3027.5	0.066	3694.2	0.044	4920.4	0.211	6172.0	0.275	
3044.6	0.082	3719.9	0.064	4960.8	0.311	6217.3	0.381	
3061.7	0.098	3745.5	0.092	5001.3	0.429	6262.6	0.479	
3078.8	0.115	3771.2	0.148	5041.7	0.553	6308.0	0.571	
3095.9	0.133	3796.8	0.232	5082.2	0.675	6353.3	0.659	
3113.0	0.152	3822.5	0.325	5122.6	0.788	6398.6	0.738	
3130.1	0.172	3848.1	0.419	5163.0	0.879	6444.0	0.804	
3147.2	0.192	3873.8	0.510	5203.5	0.943	6489.3	0.859	
3164.3	0.212	3899.4	0.599	5243.9	0.983	6534.6	0.906	
3181.5	0.234	3925.0	0.688	5284.4	1.000	6580.0	0.946	
3198.6	0.256	3950.7	0.763	5324.8	0.993	6625.3	0.975	
3215.7	0.279	3976.3	0.810	5365.3	0.975	6670.6	0.990	
3232.8	0.302	4002.0	0.839	5405.7	0.949	6716.0	0.998	
3249.9	0.325	4027.6	0.869	5446.1	0.915	6761.3	1.000	
3267.0	0.349	4053.3	0.895	5486.6	0.877	6806.6	0.998	
3284.1	0.373	4078.9	0.916	5527.0	0.835	6851.9	0.995	
3301.2	0.398	4104.6	0.936	5567.5	0.790	6897.3	0.992	
3318.3	0.423	4130.2	0.954	5607.9	0.742	6942.6	0.985	
3335.4	0.449	4155.9	0.967	5648.4	0.694	6987.9	0.974	
3352.5	0.475	4181.5	0.977	5688.8	0.648	7033.3	0.959	
3369.6	0.501	4207.2	0.985	5729.2	0.605	7078.6	0.943	
3386.7	0.528	4232.8	0.992	5769.7	0.565	7123.9	0.926	
3403.8	0.556	4258.5	0.996	5810.1	0.525	7169.3	0.909	
3420.9	0.583	4284.1	0.999	5850.6	0.486	7214.6	0.891	
3438.0	0.611	4309.8	1.000	5891.0	0.446	7259.9	0.873	
3455.1	0.639	4335.4	0.998	5931.4	0.407	7305.3	0.853	
3472.2	0.667	4361.1	0.991	5971.9	0.370	7350.6	0.832	
3489.3	0.695	4386.7	0.981	6012.3	0.334	7395.9	0.809	
3506.4	0.722	4412.3	0.970	6052.8	0.301	7441.2	0.783	
3523.5	0.749	4438.0	0.954	6093.2	0.270	7486.6	0.752	
3540.6	0.775	4463.6	0.933	6133.7	0.240	7531.9	0.717	
3557.8	0.800	4489.3	0.910	6174.1	0.214	7577.2	0.680	
3574.9	0.824	4514.9	0.887	6214.5	0.189	7622.6	0.644	
3592.0	0.847	4540.6	0.865	6255.0	0.167	7667.9	0.608	
3609.1	0.870	4566.2	0.843	6295.4	0.146	7713.2	0.573	
3626.2	0.892	4591.9	0.821	6335.9	0.128	7758.6	0.537	
3643.3	0.913	4617.5	0.797	6376.3	0.111	7803.9	0.502	
3660.4	0.933	4643.2	0.772	6416.7	0.096	7849.2	0.466	
3677.5	0.952	4668.8	0.746	6457.2	0.082	7894.5	0.430	
3694.6	0.970	4694.5	0.719	6497.6	0.069	7939.9	0.394	
3711.7	0.985	4720.1	0.691	6538.1	0.058	7985.2	0.357	
3728.8	0.996	4745.8	0.660	6578.5	0.047	8030.5	0.320	
3745.9	1.000	4771.4	0.628	6619.0	0.038	8075.9	0.285	
3763.0	0.997	4797.1	0.595	6659.4	0.030	8121.2	0.252	
3780.1	0.985	4822.7	0.564	6699.8	0.024	8166.5	0.223	
3797.2	0.962	4848.3	0.533	6740.3	0.019	8211.9	0.198	
3814.3	0.929	4874.0	0.502	6780.7	0.015	8257.2	0.176	
3831.4	0.885	4899.6	0.471	6821.2	0.012	8302.5	0.156	
3848.5	0.830	4925.3	0.440	6861.6	0.010	8347.9	0.136	
3865.6	0.767	4950.9	0.410	6902.1	0.008	8393.2	0.114	
3882.7	0.697	4976.6	0.378	6942.5	0.007	8438.5	0.092	
3899.8	0.625	5002.2	0.347	6982.9	0.006	8483.8	0.074	
3917.0	0.552	5027.9	0.316	7023.4	0.006	8529.2	0.062	
3934.1	0.481	5053.5	0.284	7063.8	0.005	8574.5	0.052	
3951.2	0.413	5079.2	0.253	7104.3	0.004	8619.8	0.044	
3968.3	0.349	5104.8	0.226	7144.7	0.004	8665.2	0.038	
3985.4	0.290	5130.5	0.204	7185.1	0.003	8710.5	0.031	
4002.5	0.238	5156.1	0.182	7225.6	0.003	8755.8	0.025	
4019.6	0.191	5181.8	0.160	7266.0	0.003	8801.2	0.021	
4036.7	0.151	5207.4	0.138	7306.5	0.002	8846.5	0.018	
4053.8	0.117	5233.1	0.116	7346.9	0.002	8891.8	0.014	
4070.9	0.089	5258.7	0.094	7387.4	0.002	8937.2	0.012	
4088.0	0.066	5284.4	0.074	7427.8	0.001	8982.5	0.010	
4105.1	0.047	5310.0	0.057	7468.2	0.001	9027.8	0.008	
4122.2	0.033	5335.6	0.041	7508.7	0.001	9073.1	0.006	
4139.3	0.022	5361.3	0.026	7549.1	0.001	9118.5	0.005	
4156.4	0.013	5386.9	0.016	7589.6	0.000	9163.8	0.003	
4173.5	0.008	5412.6	0.010	7630.0	0.000	9209.1	0.003	
4190.6	0.003	5438.2	0.005	7670.4	0.000	9254.5	0.002	

**Table 4**  
 Energy  
 Response  
 Functions,  
 $S_x(\lambda)$ , for Cape

$\lambda$	$U$
Å	Trans
3190.4	0.000
3215.4	0.003
3240.3	0.006
3265.3	0.009
3290.3	0.012
3315.3	0.014
3340.3	0.017
3365.3	0.021
3390.2	0.030
3415.2	0.043
3440.2	0.065
3465.2	0.098
3490.2	0.139
3515.2	0.188
3540.1	0.246
3565.1	0.309
3590.1	0.379
3615.1	0.452
3640.1	0.527
3665.1	0.604
3690.0	0.679
3715.0	0.751
3740.0	0.820
3765.0	0.880
3790.0	0.931
3814.9	0.969
3839.9	0.991
3864.9	1.000
3889.9	0.986
3914.9	0.950
3939.9	0.897
3964.8	0.820
3989.8	0.726
4014.8	0.626
4039.8	0.522
4064.8	0.422
4089.8	0.339
4114.7	0.275
4139.7	0.222
4164.7	0.186
4189.7	0.163
4214.7	0.143
4239.7	0.129
4264.6	0.118
4289.6	0.109
4314.6	0.102
4339.6	0.096
4364.6	0.091
4389.6	0.088
4414.5	0.086
4439.5	0.085
4464.5	0.086
4489.5	0.088
4514.5	0.092
4539.5	0.097
4564.4	0.101
4589.4	0.106
4614.4	0.110
4639.4	0.113
4664.4	0.114
4689.3	0.113
4714.3	0.110
4739.3	0.105
4764.3	0.098
4789.3	0.090
4814.3	0.080
4839.2	0.070
4864.2	0.059
4889.2	0.048
4914.2	0.039
4939.2	0.030
4964.2	0.022
4989.1	0.014
5014.1	0.007

**Table 5**  
Energy Response Functions,  $S_x(\lambda)$ , for DDO

$m35$		$m38$		$m41$		$m42$		$m45$		$m48$	
$\lambda$	Trans										
Å		Å		Å		Å		Å		Å	
3166.1	0.000	3605.5	0.000	4094.0	0.000	4199.0	0.000	4454.2	0.000	4695.1	0.000
3176.1	0.004	3613.0	0.011	4096.4	0.002	4200.7	0.003	4455.9	0.004	4700.8	0.008
3186.1	0.008	3620.6	0.024	4098.8	0.004	4202.3	0.005	4457.6	0.008	4706.4	0.013
3196.1	0.017	3628.1	0.041	4101.2	0.006	4204.0	0.010	4459.2	0.013	4712.1	0.016
3206.1	0.030	3635.6	0.063	4103.6	0.010	4205.7	0.016	4460.9	0.019	4717.7	0.019
3216.1	0.047	3643.2	0.090	4106.0	0.015	4207.3	0.023	4462.6	0.026	4723.4	0.023
3226.1	0.071	3650.7	0.121	4108.4	0.022	4209.0	0.030	4464.2	0.035	4729.0	0.028
3236.1	0.102	3658.2	0.158	4110.8	0.030	4210.6	0.037	4465.9	0.048	4734.7	0.035
3246.1	0.137	3665.8	0.200	4113.3	0.039	4212.3	0.050	4467.6	0.066	4740.3	0.044
3256.1	0.181	3673.3	0.246	4115.7	0.051	4214.0	0.074	4469.2	0.094	4746.0	0.056
3266.1	0.228	3680.8	0.295	4118.1	0.067	4215.6	0.105	4470.9	0.131	4751.6	0.068
3276.1	0.279	3688.4	0.346	4120.5	0.089	4217.3	0.145	4472.6	0.182	4757.3	0.084
3286.1	0.332	3695.9	0.399	4122.9	0.117	4219.0	0.194	4474.2	0.248	4762.9	0.104
3296.1	0.386	3703.4	0.451	4125.3	0.153	4220.6	0.252	4475.9	0.322	4768.6	0.130
3306.1	0.443	3711.0	0.504	4127.7	0.196	4222.3	0.324	4477.6	0.402	4774.2	0.161
3316.1	0.501	3718.5	0.554	4130.1	0.246	4223.9	0.408	4479.2	0.487	4779.9	0.202
3326.1	0.555	3726.0	0.603	4132.5	0.309	4225.6	0.497	4480.9	0.576	4785.5	0.254
3336.1	0.606	3733.5	0.650	4134.9	0.387	4227.3	0.589	4482.5	0.670	4791.1	0.317
3346.1	0.653	3741.1	0.695	4137.3	0.477	4228.9	0.681	4484.2	0.762	4796.8	0.394
3356.1	0.699	3748.6	0.737	4139.7	0.563	4230.6	0.766	4485.9	0.831	4802.4	0.482
3366.1	0.742	3756.1	0.776	4142.1	0.645	4232.3	0.842	4487.5	0.880	4808.1	0.575
3376.1	0.782	3763.7	0.813	4144.6	0.723	4233.9	0.906	4489.2	0.916	4813.7	0.669
3386.1	0.817	3771.2	0.845	4147.0	0.798	4235.6	0.941	4490.9	0.935	4819.4	0.757
3396.1	0.848	3778.7	0.873	4149.4	0.864	4237.2	0.958	4492.5	0.945	4825.0	0.835
3406.2	0.877	3786.3	0.898	4151.8	0.911	4238.9	0.968	4494.2	0.951	4830.7	0.894
3416.2	0.905	3793.8	0.921	4154.2	0.943	4240.6	0.969	4495.9	0.954	4836.3	0.938
3426.2	0.930	3801.3	0.941	4156.6	0.963	4242.2	0.966	4497.5	0.957	4842.0	0.968
3436.2	0.948	3808.9	0.958	4159.0	0.972	4243.9	0.962	4499.2	0.962	4847.6	0.984
3446.2	0.960	3816.4	0.971	4161.4	0.978	4245.5	0.958	4500.9	0.969	4853.3	0.994
3456.2	0.970	3823.9	0.982	4163.8	0.983	4247.2	0.954	4502.5	0.976	4858.9	0.999
3466.2	0.980	3831.5	0.990	4166.2	0.987	4248.9	0.952	4504.2	0.984	4864.6	1.000
3476.2	0.988	3839.0	0.995	4168.6	0.990	4250.5	0.953	4505.9	0.991	4870.2	1.000
3486.2	0.994	3846.5	0.999	4171.0	0.993	4252.2	0.956	4507.5	0.996	4875.9	0.999
3496.2	0.998	3854.0	1.000	4173.4	0.995	4253.9	0.963	4509.2	0.999	4881.5	0.998
3506.2	1.000	3861.6	0.999	4175.9	0.997	4255.5	0.971	4510.9	1.000	4887.1	0.997
3516.2	1.000	3869.1	0.996	4178.3	0.998	4257.2	0.979	4512.5	0.996	4892.8	0.996
3526.2	0.999	3876.6	0.992	4180.7	0.999	4258.8	0.984	4514.2	0.989	4898.4	0.995
3536.2	0.995	3884.2	0.986	4183.1	1.000	4260.5	0.990	4515.8	0.981	4904.1	0.994
3546.2	0.988	3891.7	0.977	4185.5	1.000	4262.2	0.994	4517.5	0.973	4909.7	0.993
3556.2	0.979	3899.2	0.966	4187.9	0.999	4263.8	0.999	4519.2	0.964	4915.4	0.992
3566.2	0.969	3906.8	0.950	4190.3	0.998	4265.5	1.000	4520.8	0.956	4921.0	0.991
3576.2	0.956	3914.3	0.932	4192.7	0.996	4267.1	0.998	4522.5	0.950	4926.7	0.991
3586.2	0.941	3921.8	0.909	4195.1	0.995	4268.8	0.994	4524.2	0.944	4932.3	0.990
3596.2	0.923	3929.4	0.882	4197.5	0.993	4270.5	0.983	4525.8	0.942	4938.0	0.988
3606.2	0.903	3936.9	0.852	4199.9	0.990	4272.1	0.968	4527.5	0.942	4943.6	0.987
3616.2	0.881	3944.4	0.820	4202.3	0.986	4273.8	0.946	4529.2	0.940	4949.3	0.986
3626.2	0.857	3952.0	0.788	4204.7	0.981	4275.5	0.915	4530.8	0.937	4954.9	0.983
3636.2	0.830	3959.5	0.758	4207.2	0.974	4277.1	0.878	4532.5	0.931	4960.6	0.977
3646.2	0.800	3967.0	0.725	4209.6	0.962	4278.8	0.836	4534.2	0.916	4966.2	0.969
3656.3	0.768	3974.5	0.686	4212.0	0.932	4280.4	0.788	4535.8	0.891	4971.9	0.955
3666.3	0.733	3982.1	0.643	4214.4	0.886	4282.1	0.734	4537.5	0.852	4977.5	0.934
3676.3	0.697	3989.6	0.601	4216.8	0.824	4283.8	0.669	4539.2	0.786	4983.1	0.903
3686.3	0.660	3997.1	0.559	4219.2	0.752	4285.4	0.595	4540.8	0.698	4988.8	0.866
3696.3	0.620	4004.7	0.517	4221.6	0.671	4287.1	0.522	4542.5	0.606	4994.4	0.822
3706.3	0.576	4012.2	0.475	4224.0	0.582	4288.8	0.454	4544.2	0.508	5000.1	0.762
3716.3	0.530	4019.7	0.433	4226.4	0.492	4290.4	0.389	4545.8	0.412	5005.7	0.687
3726.3	0.482	4027.3	0.392	4228.8	0.405	4292.1	0.325	4547.5	0.328	5011.4	0.609
3736.3	0.432	4034.8	0.352	4231.2	0.325	4293.7	0.265	4549.1	0.259	5017.0	0.532
3746.3	0.383	4042.3	0.312	4233.6	0.257	4295.4	0.210	4550.8	0.199	5022.7	0.457
3756.3	0.336	4049.9	0.271	4236.0	0.203	4297.1	0.168	4552.5	0.151	5028.3	0.385
3766.3	0.290	4057.4	0.234	4238.5	0.161	4298.7	0.135	4554.1	0.114	5034.0	0.323
3776.3	0.246	4064.9	0.201	4240.9	0.130	4300.4	0.108	4555.8	0.085	5039.6	0.270
3786.3	0.207	4072.5	0.172	4243.3	0.107	4302.0	0.087	4557.5	0.066	5045.3	0.226
3796.3	0.170	4080.0	0.145	4245.7	0.088	4303.7	0.070	4559.1	0.052	5050.9	0.189
3806.3	0.137	4087.5	0.121	4248.1	0.071	4305.4	0.057	4560.8	0.041	5056.6	0.160
3816.3	0.106	4095.0	0.099	4250.5	0.056	4307.0	0.046	4562.5	0.033	5062.2	0.135
3826.3	0.080	4102.6	0.080	4252.9	0.042	4308.7	0.036	4564.1	0.027	5067.9	0.114
3836.3	0.058	4110.1	0.063	4255.3	0.031	4310.4	0.028	4565.8	0.022	5073.5	0.094
3846.3	0.039	4117.6	0.048	4257.7	0.022	4312.0	0.021	4567.5	0.018	5079.1	0.078
3856.3	0.025	4125.2	0.036	4260.1	0.017	4313.7	0.015	4569.1	0.014	5084.8	0.065
3866.3	0.015	4132.7	0.026	4262.5	0.012	4315.3	0.011	4570.8	0.010	5090.4	0.052
3876.3	0.009	4140.2	0.017	4264.9	0.009	4317.0	0.008	4572.5	0.007	5096.1	0.040
3886.3	0.004	4147.8	0.011	4267.3	0.006	4318.7	0.005	4574.1	0.004	5101.7	0.026
3896.4	0.002	4155.3	0.005	4269.8	0.003	4320.3	0.002	4575.8	0.002	5107.4	0.013

**Table 6**  
 Energy Response Functions,  
 $S_x(\lambda)$ , for Eggen

$\lambda$	<i>R</i>		<i>I</i>	
	Å	Trans	λ	Å
5010.7	0.000		7309.7	0.000
5071.3	0.001		7349.2	0.004
5131.9	0.004		7388.6	0.009
5192.5	0.012		7428.0	0.019
5253.1	0.026		7467.4	0.034
5313.7	0.055		7506.8	0.055
5374.3	0.116		7546.3	0.083
5434.9	0.221		7585.7	0.118
5495.5	0.379		7625.1	0.164
5556.1	0.529		7664.5	0.236
5616.7	0.618		7704.0	0.353
5677.3	0.677		7743.4	0.529
5737.9	0.721		7782.8	0.699
5798.5	0.752		7822.2	0.805
5859.1	0.777		7861.7	0.863
5919.7	0.799		7901.1	0.909
5980.3	0.818		7940.5	0.943
6040.9	0.836		7979.9	0.967
6101.5	0.852		8019.4	0.985
6162.1	0.865		8058.8	0.995
6222.7	0.876		8098.2	0.999
6283.2	0.888		8137.6	1.000
6343.8	0.899		8177.1	0.997
6404.4	0.910		8216.5	0.990
6465.0	0.919		8255.9	0.977
6525.6	0.928		8295.3	0.958
6586.2	0.938		8334.8	0.936
6646.8	0.948		8374.2	0.913
6707.4	0.956		8413.6	0.887
6768.0	0.964		8453.0	0.861
6828.6	0.972		8492.4	0.835
6889.2	0.978		8531.9	0.810
6949.8	0.984		8571.3	0.785
7010.4	0.990		8610.7	0.761
7071.0	0.995		8650.1	0.737
7131.6	0.997		8689.6	0.712
7192.2	0.998		8729.0	0.689
7252.8	0.999		8768.4	0.666
7313.4	0.999		8807.8	0.646
7374.0	1.000		8847.3	0.630
7434.6	1.000		8886.7	0.616
7495.2	0.997		8926.1	0.603
7555.8	0.993		8965.5	0.591
7616.4	0.987		9005.0	0.578
7677.0	0.981		9044.4	0.562
7737.5	0.974		9083.8	0.545
7798.1	0.963		9123.2	0.528
7858.7	0.948		9162.7	0.509
7919.3	0.926		9202.1	0.488
7979.9	0.897		9241.5	0.465
8040.5	0.854		9280.9	0.442
8101.1	0.787		9320.3	0.413
8161.7	0.700		9359.8	0.378
8222.3	0.603		9399.2	0.341
8282.9	0.505		9438.6	0.301
8343.5	0.417		9478.0	0.261
8404.1	0.344		9517.5	0.222
8464.7	0.289		9556.9	0.186
8525.3	0.250		9596.3	0.157
8585.9	0.223		9635.7	0.135
8646.5	0.203		9675.2	0.118
8707.1	0.187		9714.6	0.102
8767.7	0.173		9754.0	0.087
8828.3	0.159		9793.4	0.073
8888.9	0.143		9832.9	0.062
8949.5	0.129		9872.3	0.051
9010.1	0.115		9911.7	0.040
9070.7	0.102		9951.1	0.029
9131.2	0.088		9990.6	0.021
9191.8	0.074		10030.0	0.015
9252.4	0.060		10069.4	0.011
9313.0	0.046		10108.8	0.007
9373.6	0.031		10148.3	0.005
9434.2	0.016		10187.7	0.002

**Table 7**  
Energy Response Functions,  $S_x(\lambda)$ , for Geneva

$\lambda$	U Å	B1		B		B2		V1		V		G	
		Trans	$\lambda$ Å										
2909.4	0.000	3533.3	0.000	3580.5	0.000	4115.7	0.000	4972.4	0.000	4838.4	0.000	5498.3	0.000
2923.5	0.018	3550.3	0.001	3600.8	0.018	4125.1	0.004	4991.0	0.058	4864.2	0.023	5508.8	0.029
2937.6	0.036	3567.3	0.002	3621.2	0.036	4134.4	0.008	5009.6	0.116	4890.0	0.046	5519.4	0.059
2951.7	0.054	3584.4	0.003	3641.6	0.055	4143.8	0.012	5028.2	0.175	4915.7	0.071	5530.0	0.090
2965.9	0.072	3601.4	0.004	3661.9	0.076	4153.2	0.016	5046.8	0.233	4941.5	0.121	5540.5	0.123
2980.0	0.090	3618.5	0.006	3682.3	0.109	4162.5	0.020	5065.3	0.300	4967.3	0.213	5551.1	0.160
2994.1	0.108	3635.5	0.016	3702.6	0.157	4171.9	0.025	5083.9	0.389	4993.1	0.333	5561.6	0.211
3008.2	0.127	3652.6	0.038	3723.0	0.210	4181.2	0.032	5102.5	0.500	5018.9	0.457	5572.2	0.285
3022.4	0.148	3669.6	0.062	3743.4	0.264	4190.6	0.045	5121.1	0.613	5044.7	0.572	5582.7	0.377
3036.5	0.174	3686.7	0.087	3763.7	0.321	4200.0	0.064	5139.7	0.726	5070.5	0.666	5593.3	0.476
3050.6	0.203	3703.7	0.110	3784.1	0.383	4209.3	0.085	5158.2	0.832	5096.3	0.745	5603.8	0.580
3064.8	0.233	3720.8	0.139	3804.5	0.449	4218.7	0.105	5176.8	0.903	5122.1	0.824	5614.4	0.683
3078.9	0.262	3737.8	0.188	3824.8	0.517	4228.0	0.127	5195.4	0.934	5147.9	0.892	5625.0	0.770
3093.0	0.292	3754.8	0.257	3845.2	0.585	4237.4	0.148	5214.0	0.954	5173.7	0.933	5635.5	0.829
3107.1	0.321	3771.9	0.329	3865.6	0.647	4246.8	0.175	5232.5	0.974	5199.5	0.956	5646.1	0.869
3121.3	0.351	3788.9	0.399	3885.9	0.700	4256.1	0.216	5251.1	0.993	5225.2	0.977	5656.6	0.904
3135.4	0.381	3806.0	0.468	3906.3	0.745	4265.5	0.273	5269.7	0.999	5251.0	0.994	5667.2	0.938
3149.5	0.412	3823.0	0.536	3926.6	0.790	4274.9	0.332	5288.3	0.988	5276.8	1.000	5677.7	0.971
3163.7	0.443	3840.1	0.605	3947.0	0.835	4284.2	0.393	5306.9	0.969	5302.6	0.996	5688.3	0.993
3177.8	0.474	3857.1	0.674	3967.4	0.870	4293.6	0.455	5325.4	0.949	5328.4	0.992	5698.9	1.000
3191.9	0.506	3874.2	0.742	3987.7	0.896	4302.9	0.519	5344.0	0.929	5354.2	0.986	5709.4	0.995
3206.0	0.537	3891.2	0.809	4008.1	0.918	4312.3	0.581	5362.6	0.906	5380.0	0.973	5720.0	0.986
3220.2	0.569	3908.3	0.872	4028.5	0.940	4321.7	0.637	5381.2	0.878	5405.8	0.956	5730.5	0.976
3234.3	0.601	3925.3	0.920	4048.8	0.961	4331.0	0.685	5399.7	0.846	5431.6	0.938	5741.1	0.965
3248.4	0.632	3942.3	0.947	4069.2	0.974	4340.4	0.733	5418.3	0.813	5457.4	0.919	5751.6	0.950
3262.5	0.662	3959.4	0.961	4089.5	0.982	4349.7	0.781	5436.9	0.780	5483.2	0.897	5762.2	0.931
3276.7	0.690	3976.4	0.976	4109.9	0.990	4359.1	0.831	5455.5	0.747	5509.0	0.873	5772.7	0.909
3290.8	0.719	3993.5	0.989	4130.3	0.997	4368.5	0.882	5474.1	0.712	5534.7	0.848	5783.3	0.885
3304.9	0.748	4010.5	1.000	4150.6	1.000	4377.8	0.928	5492.6	0.676	5560.5	0.823	5793.9	0.860
3319.1	0.778	4027.6	0.990	4171.0	0.996	4387.2	0.955	5511.2	0.639	5586.3	0.796	5804.4	0.835
3333.2	0.807	4044.6	0.959	4191.4	0.989	4396.5	0.964	5529.8	0.602	5612.1	0.767	5815.0	0.809
3347.3	0.836	4061.7	0.923	4211.7	0.981	4405.9	0.973	5548.4	0.565	5637.9	0.738	5825.5	0.782
3361.4	0.864	4078.7	0.888	4232.1	0.972	4415.3	0.981	5567.0	0.529	5663.7	0.709	5836.1	0.755
3375.6	0.885	4095.8	0.853	4252.4	0.960	4424.6	0.989	5585.5	0.493	5689.5	0.679	5846.6	0.726
3389.7	0.901	4112.8	0.813	4272.8	0.944	4434.0	0.997	5604.1	0.458	5715.3	0.649	5857.2	0.697
3403.8	0.916	4129.8	0.758	4293.2	0.926	4443.4	1.000	5622.7	0.423	5741.1	0.618	5867.8	0.667
3417.9	0.932	4146.9	0.692	4313.5	0.908	4452.7	0.990	5641.3	0.388	5766.9	0.587	5878.3	0.638
3432.1	0.948	4163.9	0.625	4333.9	0.890	4462.1	0.971	5659.8	0.354	5792.7	0.555	5888.9	0.609
3446.2	0.964	4181.0	0.560	4354.3	0.871	4471.4	0.951	5678.4	0.323	5818.5	0.525	5899.4	0.579
3460.3	0.979	4198.0	0.495	4374.6	0.851	4480.8	0.931	5697.0	0.293	5844.2	0.494	5910.0	0.549
3474.5	0.994	4215.1	0.439	4395.0	0.832	4490.2	0.910	5715.6	0.263	5870.0	0.463	5920.5	0.517
3488.6	0.999	4232.1	0.393	4415.3	0.811	4499.5	0.888	5734.2	0.234	5895.8	0.433	5931.1	0.487
3502.7	0.997	4249.2	0.354	4435.7	0.791	4508.9	0.858	5752.7	0.206	5921.6	0.403	5941.6	0.458
3516.8	0.993	4266.2	0.316	4456.1	0.768	4518.2	0.818	5771.3	0.182	5947.4	0.375	5952.2	0.431
3531.0	0.989	4283.3	0.279	4476.4	0.745	4527.6	0.772	5789.9	0.162	5973.2	0.346	5962.8	0.404
3545.1	0.985	4300.3	0.242	4496.8	0.721	4537.0	0.725	5808.5	0.142	5999.0	0.318	5973.3	0.375
3559.2	0.980	4317.3	0.212	4517.2	0.696	4546.3	0.677	5827.1	0.123	6024.8	0.292	5983.9	0.347
3573.4	0.976	4334.4	0.187	4537.5	0.663	4555.7	0.627	5845.6	0.104	6050.6	0.267	5994.4	0.320
3587.5	0.972	4351.4	0.165	4557.9	0.622	4565.0	0.577	5864.2	0.088	6076.4	0.243	6005.0	0.296
3601.6	0.953	4368.5	0.143	4578.3	0.580	4574.4	0.529	5882.8	0.076	6102.2	0.219	6015.5	0.273
3615.7	0.918	4385.5	0.122	4598.6	0.537	4583.8	0.483	5901.4	0.066	6128.0	0.197	6026.1	0.249
3629.9	0.877	4402.6	0.102	4619.0	0.493	4593.1	0.435	5919.9	0.056	6153.7	0.177	6036.7	0.225
3644.0	0.836	4419.6	0.087	4639.3	0.447	4602.5	0.387	5938.5	0.046	6179.5	0.157	6047.2	0.202
3658.1	0.795	4436.7	0.076	4659.7	0.399	4611.9	0.338	5957.1	0.037	6205.3	0.138	6057.8	0.182
3672.2	0.754	4453.7	0.066	4680.1	0.351	4621.2	0.287	5975.7	0.031	6231.1	0.122	6068.3	0.164
3686.4	0.712	4470.8	0.055	4700.4	0.303	4630.6	0.243	5994.3	0.026	6256.9	0.107	6078.9	0.147
3700.5	0.670	4487.8	0.046	4720.8	0.262	4639.9	0.213	6012.8	0.021	6282.7	0.092	6089.4	0.129
3714.6	0.625	4504.9	0.037	4741.2	0.229	4649.3	0.190	6031.4	0.017	6308.5	0.078	6100.0	0.112
3728.8	0.573	4521.9	0.032	4761.5	0.199	4658.7	0.166	6050.0	0.013	6334.3	0.066	6110.5	0.097
3742.9	0.516	4538.9	0.027	4781.9	0.168	4668.0	0.141	6068.6	0.010	6360.1	0.057	6121.1	0.085
3757.0	0.460	4556.0	0.023	4802.2	0.139	4677.4	0.116	6087.2	0.008	6385.9	0.048	6131.7	0.074
3771.1	0.402	4573.0	0.019	4822.6	0.117	4686.7	0.093	6105.7	0.007	6411.7	0.039	6142.2	0.063
3785.3	0.345	4590.1	0.016	4843.0	0.100	4696.1	0.075	6124.3	0.005	6437.5	0.031	6152.8	0.053
3799.4	0.287	4607.1	0.013	4863.3	0.084	4705.5	0.065	6142.9	0.004	6463.2	0.026	6163.3	0.043
3813.5	0.230	4624.2	0.011	4883.7	0.068	4714.8	0.056	6161.5	0.003	6489.0	0.021	6173.9	0.035
3827.7	0.175	4641.2	0.010	4904.1	0.054	4724.2	0.046	6180.0	0.002	6514.8	0.016	6184.4	0.028
3841.8	0.137	4658.3	0.009	4924.4	0.044	4733.5	0.036	6198.6	0.002	6540.6	0.012	6195.0	0.022
3855.9	0.117	4675.3	0.008	4944.8	0.036	4742.9	0.026	6217.2	0.002	6566.4	0.009	6205.6	0.017
3870.0	0.100	4692.4	0.006	4965.1	0.027	4752.3	0.019	6235.8	0.001	6592.2	0.007	6216.1	0.011
3884.2	0.084	4709.4	0.005	4985.5	0.019	4761							

**Table 8**  
Energy Response Functions,  $S_x(\lambda)$ , for Stromgren

$\lambda$	$u$	$b$	$v$	$y$	
Å	Trans	Å	Trans	Å	Trans
3162.5	0.000	4339.1	0.000	3737.4	0.000
3171.4	0.008	4346.8	0.001	3748.3	0.002
3180.2	0.017	4354.6	0.002	3759.3	0.004
3189.1	0.029	4362.4	0.004	3770.3	0.006
3198.0	0.045	4370.1	0.005	3781.3	0.009
3206.8	0.063	4377.9	0.007	3792.3	0.011
3215.7	0.084	4385.7	0.008	3803.2	0.014
3224.6	0.109	4393.4	0.009	3814.2	0.018
3233.4	0.138	4401.2	0.011	3825.2	0.022
3242.3	0.174	4408.9	0.012	3836.2	0.026
3251.2	0.218	4416.7	0.014	3847.2	0.031
3260.0	0.264	4424.5	0.016	3858.2	0.037
3268.9	0.315	4432.2	0.017	3869.1	0.044
3277.8	0.368	4440.0	0.019	3880.1	0.052
3286.6	0.422	4447.7	0.023	3891.1	0.061
3295.5	0.476	4455.5	0.027	3902.1	0.071
3304.4	0.530	4463.3	0.032	3913.1	0.085
3313.2	0.585	4471.0	0.038	3924.0	0.102
3322.1	0.640	4478.8	0.043	3935.0	0.124
3331.0	0.692	4486.6	0.049	3946.0	0.150
3339.8	0.737	4494.3	0.055	3957.0	0.181
3348.7	0.776	4502.1	0.062	3968.0	0.220
3357.6	0.811	4509.8	0.069	3979.0	0.267
3366.4	0.843	4517.6	0.079	3989.9	0.324
3375.3	0.873	4525.4	0.091	4000.9	0.390
3384.2	0.899	4533.1	0.108	4011.9	0.464
3393.0	0.922	4540.9	0.130	4022.9	0.543
3401.9	0.942	4548.6	0.158	4033.9	0.625
3410.8	0.958	4556.4	0.190	4044.8	0.707
3419.7	0.971	4564.2	0.231	4055.8	0.782
3428.5	0.982	4571.9	0.279	4066.8	0.845
3437.4	0.988	4579.7	0.336	4077.8	0.898
3446.3	0.991	4587.5	0.401	4088.8	0.938
3455.1	0.994	4595.2	0.473	4099.8	0.968
3464.0	0.997	4603.0	0.549	4110.7	0.988
3472.9	1.000	4610.7	0.628	4121.7	0.998
3481.7	0.999	4618.5	0.708	4132.7	0.997
3490.6	0.994	4626.3	0.782	4143.7	0.982
3499.5	0.987	4634.0	0.844	4154.7	0.950
3508.3	0.981	4641.8	0.895	4165.6	0.903
3517.2	0.974	4649.6	0.935	4176.6	0.842
3526.1	0.967	4657.3	0.966	4187.6	0.767
3534.9	0.961	4665.1	0.988	4198.6	0.685
3543.8	0.953	4672.8	0.999	4209.6	0.600
3552.7	0.941	4680.6	0.997	4220.6	0.516
3561.5	0.920	4688.4	0.982	4231.5	0.441
3570.4	0.893	4696.1	0.950	4242.5	0.377
3579.3	0.867	4703.9	0.903	4253.5	0.323
3588.1	0.840	4711.6	0.844	4264.5	0.276
3597.0	0.812	4719.4	0.774	4275.5	0.235
3605.9	0.780	4727.2	0.697	4286.4	0.199
3614.7	0.743	4734.9	0.617	4297.4	0.167
3623.6	0.706	4742.7	0.536	4308.4	0.138
3632.5	0.669	4750.5	0.457	4319.4	0.116
3641.3	0.631	4758.2	0.384	4330.4	0.098
3650.2	0.589	4766.0	0.318	4341.4	0.084
3659.1	0.543	4773.7	0.263	4352.3	0.071
3667.9	0.495	4781.5	0.220	4363.3	0.061
3676.8	0.447	4789.3	0.187	4374.3	0.052
3685.7	0.397	4797.0	0.162	4385.3	0.047
3694.6	0.350	4804.8	0.142	4396.3	0.043
3703.4	0.306	4812.5	0.125	4407.2	0.040
3712.3	0.265	4820.3	0.108	4418.2	0.037
3721.2	0.228	4828.1	0.092	4429.2	0.034
3730.0	0.195	4835.8	0.078	4440.2	0.031
3738.9	0.165	4843.6	0.066	4451.2	0.029
3747.8	0.134	4851.4	0.056	4462.2	0.026
3756.6	0.104	4859.1	0.047	4473.1	0.022
3765.5	0.075	4866.9	0.040	4484.1	0.018
3774.4	0.054	4874.6	0.032	4495.1	0.015
3783.2	0.041	4882.4	0.024	4506.1	0.011
3792.1	0.031	4890.2	0.016	4517.1	0.009
3801.0	0.021	4897.9	0.010	4528.1	0.006
3809.8	0.010	4905.7	0.006	4539.0	0.003

**Table 9**  
Energy Response Functions,  $S_x(\lambda)$ , for Vilnius

$\lambda$	$U$	$P$	$X$	$Y$	$Z$	$V$	$S$
Å	Trans	Å	Trans	Å	Trans	Å	Trans
3047.3	0.000	3533.8	0.000	3674.0	0.000	4346.0	0.000
3057.6	0.002	3539.5	0.003	3686.7	0.005	4360.0	0.022
3067.9	0.003	3545.1	0.006	3699.5	0.009	4373.9	0.044
3078.2	0.005	3550.8	0.009	3712.2	0.014	4387.9	0.067
3088.4	0.008	3556.5	0.013	3725.0	0.020	4401.9	0.101
3098.7	0.012	3562.1	0.016	3737.7	0.029	4415.9	0.157
3109.0	0.018	3567.8	0.022	3750.5	0.039	4429.8	0.236
3119.3	0.025	3573.5	0.030	3763.3	0.050	4443.8	0.325
3129.5	0.032	3579.1	0.038	3776.0	0.063	4457.8	0.416
3139.8	0.041	3584.8	0.047	3788.8	0.081	4471.8	0.505
3150.1	0.052	3590.5	0.057	3801.5	0.104	4485.7	0.591
3160.4	0.066	3596.1	0.068	3814.3	0.126	4499.7	0.676
3170.6	0.080	3601.8	0.085	3827.0	0.152	4513.7	0.760
3180.9	0.095	3607.4	0.107	3839.8	0.186	4527.7	0.835
3191.2	0.113	3613.1	0.129	3852.6	0.226	4541.6	0.893
3201.5	0.134	3618.8	0.152	3865.3	0.268	4555.6	0.929
3211.7	0.157	3624.4	0.176	3878.1	0.312	4569.6	0.957
3222.0	0.180	3630.1	0.204	3890.8	0.361	4583.6	0.982
3232.3	0.205	3635.8	0.238	3903.6	0.415	4597.5	0.997
3242.6	0.234	3641.4	0.274	3916.3	0.470	4611.5	0.998
3252.8	0.264	3647.1	0.310	3929.1	0.526	4625.5	0.990
3263.1	0.295	3652.8	0.348	3941.9	0.585	4639.5	0.978
3273.4	0.327	3658.4	0.387	3954.6	0.646	4653.4	0.962
3283.7	0.361	3664.1	0.429	3967.4	0.709	4667.4	0.939
3293.9	0.396	3669.7	0.473	3980.1	0.771	4681.4	0.907
3304.2	0.432	3675.4	0.519	3992.9	0.827	4695.3	0.871
3314.5	0.470	3681.1	0.566	4005.6	0.876	4709.3	0.833
3324.8	0.507	3686.7	0.613	4018.4	0.924	4723.3	0.795
3335.0	0.545	3692.4	0.658	4031.2	0.969	4737.3	0.755
3345.3	0.583	3698.1	0.700	4043.9	0.996	4751.2	0.714
3355.6	0.623	3703.7	0.743	4056.7	0.999	4765.2	0.673
3365.9	0.660	3709.4	0.785	4069.4	0.995	4779.2	0.631
3376.1	0.695	3715.1	0.828	4082.2	0.990	4793.2	0.592
3386.4	0.728	3720.7	0.867	4094.9	0.945	4807.1	0.554
3396.7	0.762	3726.4	0.897	4107.7	0.859	4821.1	0.517
3407.0	0.795	3732.0	0.921	4120.4	0.755	4835.1	0.480
3417.2	0.825	3737.7	0.945	4133.2	0.650	4849.1	0.443
3427.5	0.851	3743.4	0.969	4146.0	0.551	4863.0	0.409
3437.8	0.878	3749.0	0.990	4158.7	0.461	4877.0	0.377
3448.1	0.905	3754.7	0.999	4171.5	0.376	4891.0	0.345
3458.3	0.929	3760.4	0.998	4184.2	0.290	4905.0	0.314
3468.6	0.948	3766.0	0.995	4197.0	0.219	4918.9	0.286
3478.9	0.966	3771.7	0.991	4209.7	0.178	4932.9	0.262
3489.2	0.985	3777.4	0.984	4222.5	0.151	4946.9	0.241
3499.4	0.997	3783.0	0.964	4235.3	0.124	4960.9	0.222
3509.7	0.999	3788.7	0.926	4248.0	0.101	4974.8	0.203
3520.0	0.996	3794.3	0.881	4260.8	0.086	4988.8	0.186
3530.3	0.992	3800.0	0.836	4273.5	0.075	5002.8	0.172
3540.5	0.985	3805.7	0.789	4286.3	0.065	5016.8	0.160
3550.8	0.969	3811.3	0.736	4299.0	0.057	5030.7	0.148
3561.1	0.946	3817.0	0.675	4311.8	0.052	5044.7	0.136
3571.4	0.921	3822.7	0.609	4324.6	0.051	5058.7	0.126
3581.6	0.894	3828.3	0.541	4337.3	0.050	5072.7	0.116
3591.9	0.856	3834.0	0.473	4350.1	0.050	5086.6	0.107
3602.2	0.807	3839.7	0.408	4362.8	0.053	5100.6	0.098
3612.5	0.753	3845.3	0.351	4375.6	0.058	5114.6	0.090
3622.7	0.697	3851.0	0.298	4388.3	0.064	5128.6	0.084
3633.0	0.636	3856.7	0.244	4401.1	0.070	5142.5	0.078
3643.3	0.569	3862.3	0.189	4413.9	0.076	5156.5	0.074
3653.6	0.497	3868.0	0.142	4426.6	0.083	5170.5	0.069
3663.8	0.423	3873.6	0.111	4439.4	0.090	5184.5	0.064
3674.1	0.354	3879.3	0.092	4452.1	0.097	5198.4	0.059
3684.4	0.296	3885.0	0.073	4464.9	0.098	5212.4	0.054
3694.7	0.247	3890.6	0.054	4477.6	0.092	5226.4	0.049
3704.9	0.197	3896.3	0.038	4490.4	0.085	5240.4	0.045
3715.2	0.150	3902.0	0.028	4503.2	0.077	5254.3	0.040
3725.5	0.113	3907.6	0.024	4515.9	0.069	5268.3	0.036
3735.8	0.089	3913.3	0.020	4528.7	0.062	5282.3	0.031
3746.0	0.067	3919.0	0.016	4541.4	0.053	5296.3	0.027
3756.3	0.044	3924.6	0.012	4554.2	0.045	5310.2	0.023
3766.6	0.028	3930.3	0.009	4566.9	0.036	5324.2	0.018
3776.9	0.019	3935.9	0.007	4579.7	0.028	5338.2	0.014
3787.1	0.013	3941.6	0.004	4592.5	0.019	5352.1	0.009
3797.4	0.006	3947.3	0.002	4605.2	0.009	5366.1	0.005

**Table 10**  
Energy Response Functions,  $S_x(\lambda)$ , for WBVR

	<i>W</i>		<i>B</i>		<i>V</i>		<i>R</i>	
$\lambda$	Trans	$\lambda$	Trans	$\lambda$	Trans	$\lambda$	Trans	
Å		Å		Å		Å		
2908.2	0.000	3486.0	0.000	4619.9	0.000	6039.9	0.000	
2923.2	0.000	3510.9	0.000	4650.4	0.001	6084.0	0.000	
2938.3	0.000	3535.8	0.000	4680.9	0.002	6128.1	0.002	
2953.3	0.001	3560.6	0.000	4711.4	0.004	6172.2	0.008	
2968.4	0.001	3585.5	0.001	4741.9	0.011	6216.3	0.037	
2983.4	0.002	3610.4	0.005	4772.4	0.023	6260.4	0.102	
2998.5	0.004	3635.2	0.013	4802.9	0.043	6304.4	0.222	
3013.5	0.006	3660.1	0.030	4833.4	0.079	6348.5	0.389	
3028.6	0.009	3685.0	0.054	4863.9	0.131	6392.6	0.570	
3043.6	0.013	3709.9	0.085	4894.3	0.199	6436.7	0.733	
3058.7	0.019	3734.7	0.121	4924.8	0.282	6480.8	0.856	
3073.7	0.025	3759.6	0.158	4955.3	0.375	6524.9	0.939	
3088.8	0.034	3784.5	0.196	4985.8	0.471	6569.0	0.983	
3103.8	0.044	3809.3	0.234	5016.3	0.562	6613.1	0.998	
3118.9	0.055	3834.2	0.273	5046.8	0.645	6657.2	0.995	
3133.9	0.068	3859.1	0.311	5077.3	0.716	6701.3	0.980	
3149.0	0.083	3884.0	0.349	5107.8	0.777	6745.4	0.959	
3164.0	0.099	3908.8	0.389	5138.3	0.830	6789.5	0.933	
3179.1	0.116	3933.7	0.428	5168.7	0.874	6833.6	0.906	
3194.1	0.133	3958.6	0.466	5199.2	0.910	6877.7	0.881	
3209.2	0.152	3983.4	0.502	5229.7	0.940	6921.8	0.856	
3224.2	0.171	4008.3	0.538	5260.2	0.963	6965.9	0.829	
3239.2	0.192	4033.2	0.573	5290.7	0.980	7010.0	0.802	
3254.3	0.213	4058.1	0.608	5321.2	0.991	7054.1	0.774	
3269.3	0.236	4082.9	0.643	5351.7	0.998	7098.2	0.747	
3284.4	0.259	4107.8	0.677	5382.2	1.000	7142.3	0.721	
3299.4	0.283	4132.7	0.709	5412.7	0.997	7186.4	0.695	
3314.5	0.308	4157.5	0.739	5443.1	0.990	7230.5	0.667	
3329.5	0.334	4182.4	0.767	5473.6	0.981	7274.6	0.641	
3344.6	0.360	4207.3	0.793	5504.1	0.969	7318.7	0.616	
3359.6	0.388	4232.2	0.817	5534.6	0.953	7362.8	0.592	
3374.7	0.416	4257.0	0.841	5565.1	0.936	7406.9	0.570	
3389.7	0.447	4281.9	0.863	5595.6	0.915	7450.9	0.548	
3404.8	0.480	4306.8	0.885	5626.1	0.889	7495.0	0.526	
3419.8	0.515	4331.6	0.906	5656.6	0.859	7539.1	0.504	
3434.9	0.553	4356.5	0.928	5687.1	0.828	7583.2	0.484	
3449.9	0.593	4381.4	0.948	5717.5	0.796	7627.3	0.466	
3465.0	0.637	4406.3	0.967	5748.0	0.761	7671.4	0.446	
3480.0	0.680	4431.1	0.982	5778.5	0.724	7715.5	0.424	
3495.1	0.723	4456.0	0.994	5809.0	0.683	7759.6	0.404	
3510.1	0.763	4480.9	1.000	5839.5	0.640	7803.7	0.386	
3525.2	0.803	4505.7	0.998	5870.0	0.597	7847.8	0.368	
3540.2	0.842	4530.6	0.989	5900.5	0.550	7891.9	0.349	
3555.3	0.878	4555.5	0.971	5931.0	0.503	7936.0	0.332	
3570.3	0.912	4580.4	0.941	5961.5	0.457	7980.1	0.315	
3585.4	0.943	4605.2	0.902	5992.0	0.417	8024.2	0.298	
3600.4	0.968	4630.1	0.854	6022.4	0.381	8068.3	0.281	
3615.5	0.985	4655.0	0.799	6052.9	0.348	8112.4	0.265	
3630.5	0.997	4679.8	0.741	6083.4	0.316	8156.5	0.249	
3645.6	0.999	4704.7	0.680	6113.9	0.287	8200.6	0.233	
3660.6	0.986	4729.6	0.617	6144.4	0.259	8244.7	0.217	
3675.6	0.962	4754.4	0.555	6174.9	0.232	8288.8	0.202	
3690.7	0.927	4779.3	0.494	6205.4	0.205	8332.9	0.186	
3705.7	0.873	4804.2	0.438	6235.9	0.180	8377.0	0.170	
3720.8	0.801	4829.1	0.387	6266.4	0.156	8421.1	0.155	
3735.8	0.716	4853.9	0.340	6296.8	0.135	8465.2	0.140	
3750.9	0.625	4878.8	0.297	6327.3	0.116	8509.3	0.126	
3765.9	0.532	4903.7	0.257	6357.8	0.099	8553.3	0.112	
3781.0	0.437	4928.5	0.217	6388.3	0.084	8597.4	0.098	
3796.0	0.343	4953.4	0.180	6418.8	0.071	8641.5	0.085	
3811.1	0.260	4978.3	0.145	6449.3	0.060	8685.6	0.072	
3826.1	0.193	5003.2	0.115	6479.8	0.050	8729.7	0.060	
3841.2	0.135	5028.0	0.090	6510.3	0.041	8773.8	0.049	
3856.2	0.086	5052.9	0.069	6540.8	0.034	8817.9	0.039	
3871.3	0.051	5077.8	0.051	6571.2	0.027	8862.0	0.030	
3886.3	0.031	5102.6	0.037	6601.7	0.022	8906.1	0.023	
3901.4	0.017	5127.5	0.026	6632.2	0.018	8950.2	0.017	
3916.4	0.007	5152.4	0.017	6662.7	0.014	8994.3	0.012	
3931.5	0.002	5177.3	0.010	6693.2	0.012	9038.4	0.009	
3946.5	0.001	5202.1	0.006	6723.7	0.009	9082.5	0.006	
3961.6	0.000	5227.0	0.003	6754.2	0.007	9126.6	0.005	
3976.6	0.000	5251.9	0.002	6784.7	0.006	9170.7	0.003	
3991.7	0.000	5276.7	0.001	6815.2	0.006	9214.8	0.002	
4006.7	0.000	5301.6	0.000	6845.6	0.004	9258.9	0.001	

**Table 11**  
 Energy Response Functions,  
 $S_x(\lambda)$ , for Cousins

<i>R</i>		<i>I</i>	
$\lambda$	Trans	$\lambda$	Trans
Å		Å	
5507.0	0.000	7028.9	0.000
5553.0	0.106	7058.8	0.025
5598.9	0.241	7088.7	0.051
5644.8	0.431	7118.6	0.083
5690.7	0.631	7148.5	0.138
5736.6	0.769	7178.4	0.210
5782.5	0.853	7208.3	0.285
5828.4	0.910	7238.2	0.366
5874.4	0.948	7268.1	0.452
5920.3	0.975	7297.9	0.540
5966.2	0.989	7327.8	0.621
6012.1	0.997	7357.7	0.691
6058.0	1.000	7387.6	0.754
6103.9	0.999	7417.5	0.812
6149.9	0.997	7447.4	0.858
6195.8	0.992	7477.3	0.890
6241.7	0.986	7507.2	0.919
6287.6	0.979	7537.1	0.944
6333.5	0.970	7567.0	0.962
6379.4	0.960	7596.9	0.976
6425.3	0.948	7626.7	0.989
6471.3	0.934	7656.6	0.995
6517.2	0.918	7686.5	0.998
6563.1	0.900	7716.4	0.999
6609.0	0.884	7746.3	1.000
6654.9	0.867	7776.2	0.999
6700.8	0.849	7806.1	0.998
6746.7	0.828	7836.0	0.997
6792.7	0.805	7865.9	0.996
6838.6	0.780	7895.8	0.995
6884.5	0.755	7925.7	0.995
6930.4	0.730	7955.6	0.995
6976.3	0.704	7985.4	0.997
7022.2	0.678	8015.3	0.998
7068.2	0.652	8045.2	0.999
7114.1	0.626	8075.1	0.998
7160.0	0.601	8105.0	0.997
7205.9	0.576	8134.9	0.995
7251.8	0.549	8164.8	0.990
7297.7	0.521	8194.7	0.985
7343.6	0.492	8224.6	0.979
7389.6	0.463	8254.5	0.974
7435.5	0.434	8284.4	0.967
7481.4	0.407	8314.3	0.961
7527.3	0.379	8344.1	0.952
7573.2	0.352	8374.0	0.942
7619.1	0.325	8403.9	0.930
7665.0	0.299	8433.8	0.918
7711.0	0.274	8463.7	0.905
7756.9	0.251	8493.6	0.892
7802.8	0.229	8523.5	0.877
7848.7	0.208	8553.4	0.859
7894.6	0.188	8583.3	0.837
7940.5	0.167	8613.2	0.815
7986.4	0.148	8643.1	0.784
8032.4	0.130	8673.0	0.743
8078.3	0.114	8702.8	0.698
8124.2	0.101	8732.7	0.649
8170.1	0.090	8762.6	0.593
8216.0	0.080	8792.5	0.530
8261.9	0.071	8822.4	0.467
8307.9	0.063	8852.3	0.404
8353.8	0.055	8882.2	0.343
8399.7	0.047	8912.1	0.282
8445.6	0.040	8942.0	0.226
8491.5	0.033	8971.9	0.178
8537.4	0.027	9001.8	0.134
8583.3	0.021	9031.7	0.094
8629.3	0.017	9061.5	0.064
8675.2	0.014	9091.4	0.043
8721.1	0.012	9121.3	0.024
8767.0	0.009	9151.2	0.010
8812.9	0.006	9181.1	0.005
8858.8	0.003	9211.0	0.003

**Table 12**  
 Energy Response Functions,  
 $S_x(\lambda)$ , for Tycho

<i>Bt</i>		<i>Vt</i>	
$\lambda$	Trans	$\lambda$	Trans
Å		Å	
3511.4	0.000	4494.7	0.000
3532.8	0.007	4525.9	0.014
3554.2	0.015	4557.2	0.042
3575.5	0.029	4588.5	0.094
3596.9	0.050	4619.7	0.175
3618.3	0.074	4651.0	0.280
3639.7	0.102	4682.3	0.399
3661.1	0.134	4713.6	0.523
3682.5	0.169	4744.8	0.638
3703.9	0.208	4776.1	0.734
3725.3	0.249	4807.4	0.807
3746.7	0.292	4838.6	0.863
3768.1	0.338	4869.9	0.901
3789.4	0.387	4901.2	0.930
3810.8	0.436	4932.4	0.953
3832.2	0.486	4963.7	0.970
3853.6	0.536	4995.0	0.983
3875.0	0.584	5026.3	0.993
3896.4	0.630	5057.5	0.998
3917.8	0.673	5088.8	1.000
3939.2	0.713	5120.1	0.998
3960.6	0.748	5151.3	0.992
3982.0	0.779	5182.6	0.982
4003.3	0.806	5213.9	0.970
4024.7	0.828	5245.2	0.955
4046.1	0.846	5276.4	0.938
4067.5	0.862	5307.7	0.920
4088.9	0.874	5339.0	0.901
4110.3	0.885	5370.2	0.881
4131.7	0.896	5401.5	0.859
4153.1	0.905	5432.8	0.837
4174.5	0.915	5464.0	0.813
4195.9	0.926	5495.3	0.789
4217.2	0.937	5526.6	0.764
4238.6	0.948	5557.9	0.739
4260.0	0.959	5589.1	0.713
4281.4	0.970	5620.4	0.687
4302.8	0.980	5651.7	0.659
4324.2	0.989	5682.9	0.631
4345.6	0.996	5714.2	0.602
4367.0	1.000	5745.5	0.573
4388.4	0.996	5776.8	0.544
4409.8	0.983	5808.0	0.515
4431.2	0.957	5839.3	0.486
4452.5	0.916	5870.6	0.457
4473.9	0.862	5901.8	0.427
4495.3	0.797	5933.1	0.398
4516.7	0.724	5964.4	0.370
4538.1	0.645	5995.7	0.343
4559.5	0.565	6026.9	0.317
4580.9	0.485	6058.2	0.291
4602.3	0.411	6089.5	0.267
4623.7	0.343	6120.7	0.245
4645.1	0.283	6152.0	0.225
4666.4	0.236	6183.3	0.207
4687.8	0.195	6214.5	0.189
4709.2	0.164	6245.8	0.172
4730.6	0.139	6277.1	0.157
4752.0	0.120	6308.4	0.143
4773.4	0.105	6339.6	0.131
4794.8	0.094	6370.9	0.120
4816.2	0.085	6402.2	0.110
4837.6	0.076	6433.4	0.100
4859.0	0.068	6464.7	0.091
4880.3	0.059	6496.0	0.082
4901.7	0.050	6527.3	0.073
4923.1	0.042	6558.5	0.065
4944.5	0.033	6589.8	0.058
4965.9	0.025	6621.1	0.050
4987.3	0.017	6652.3	0.042
5008.7	0.011	6683.6	0.033
5030.1	0.006	6714.9	0.024
5051.5	0.003	6746.2	0.016
5072.9	0.001	6777.4	0.008

**Table 13**  
 Energy  
 Response  
 Functions,  
 $S_x(\lambda)$ , for  
 Hipparcos

$\lambda$	$H_p$
$\text{\AA}$	Trans
3460.5	0.000
3540.3	0.032
3620.1	0.061
3699.9	0.097
3779.6	0.143
3859.4	0.193
3939.2	0.244
4018.9	0.301
4098.7	0.362
4178.5	0.423
4258.2	0.487
4338.0	0.558
4417.8	0.639
4497.5	0.719
4577.3	0.792
4657.1	0.858
4736.8	0.918
4816.6	0.961
4896.4	0.986
4976.1	0.998
5055.9	0.999
5135.7	0.993
5215.4	0.981
5295.2	0.964
5375.0	0.940
5454.7	0.913
5534.5	0.885
5614.3	0.856
5694.0	0.825
5773.8	0.792
5853.6	0.760
5933.3	0.728
6013.1	0.695
6092.9	0.662
6172.6	0.630
6252.4	0.598
6332.2	0.566
6411.9	0.536
6491.7	0.506
6571.5	0.478
6651.2	0.450
6731.0	0.423
6810.8	0.397
6890.5	0.371
6970.3	0.347
7050.1	0.322
7129.8	0.299
7209.6	0.275
7289.4	0.252
7369.2	0.229
7448.9	0.209
7528.7	0.189
7608.5	0.171
7688.2	0.153
7768.0	0.137
7847.8	0.122
7927.5	0.109
8007.3	0.097
8087.1	0.086
8166.8	0.076
8246.6	0.067
8326.4	0.058
8406.1	0.048
8485.9	0.040
8565.7	0.033
8645.4	0.027
8725.2	0.022
8805.0	0.018
8884.7	0.015
8964.5	0.012
9044.3	0.009
9124.0	0.006
9203.8	0.004
9283.6	0.002